Dalton Transactions

RSC Publishing

PAPER

View Article Online
View Journal | View Issue

Cite this: *Dalton Trans.*, 2013, **42**, 8468

Nuclease and anti-proliferative activities of copper(II) complexes of N_3O tripodal ligands involving a sterically hindered phenolate†

Nathalie Berthet,[a] Véronique Martel-Frachet,[b] Fabien Michel,[a] Christian Philouze,[a] Sylvain Hamman,[a] Xavier Ronot[b] and Fabrice Thomas*[a]

Received 6th November 2012,
Accepted 5th April 2013

DOI: 10.1039/c3dt32659d

www.rsc.org/dalton

Copper(II) complexes $\mathbf{1}^{2+}$–**6** of a series of tripodal ligands involving a N_3O donor set, namely 2-[(bis-pyridin-2-ylmethyl-amino)-methyl]-4-methoxy-phenol (1L), 2-*tert*-butyl-4-methoxy-6-[bis-pyridin-2-ylmethyl-amino)-methyl]-phenol (2L), 2-*tert*-butyl-4-methoxy-6-{[(2-pyridin-2-yl-ethyl)-pyridin-2-ylmethyl-amino]-methyl}-phenol (3L), 2-*tert*-butyl-4-methoxy-6-{[(6-methyl-pyridin-2-ylmethyl)-pyridin-2-ylmethyl-amino]-methyl}-phenol (4L), 2-*tert*-butyl-4-fluoro-6-{[(6-methyl-pyridin-2-ylmethyl)-pyridin-2-ylmethyl-amino]-methyl}-phenol (5L) and 2-*tert*-butyl-4-methoxy-6-{bis[(6-methyl-pyridin-2-ylmethyl)-amino]-methyl}-phenol (6L), respectively, were synthesized. Complexes $\mathbf{1}^{2+}$, $\mathbf{3}^{+}$ and $\mathbf{4}^{+}$ were structurally characterized by X-ray diffraction. The structure of $\mathbf{1}^{2+}$ is dimeric, with an essentially trigonal bipyramidal geometry around the copper(II) ions and two bridging deprotonated phenolate moieties. The mononuclear complexes $\mathbf{3}^{+}$ and $\mathbf{4}^{+}$ contain a square pyramidal copper ion, coordinated in axial position by the phenol moiety. In the water–DMF (90 : 10) mixture at pH 7.3 all the copper(II) complexes are mononuclear, mainly under their phenolate neutral form (except $\mathbf{3}^{+}$), with a coordinated solvent molecule. The DNA cleavage activity of the complexes was tested towards the ϕX174 DNA plasmid. In the absence of an exogenous agent $\mathbf{1}^{2+}$ does not show any cleavage activity, $\mathbf{2}^{+}$ and $\mathbf{3}^{+}$ are moderately active, while $\mathbf{4}^{+}$, $\mathbf{5}^{+}$ and $\mathbf{6}^{+}$ exhibit a high nuclease activity. Experiments in the presence of various scavengers reveal that reactive oxygen species (ROS) are not involved in the strand scission mechanism. The cytotoxicity of the complexes was evaluated on bladder cancer cell lines sensitive or resistant to cisplatin. The IC_{50} values of the complexes $\mathbf{2}^{+}$, $\mathbf{4}^{+}$, $\mathbf{5}^{+}$ and $\mathbf{6}^{+}$ are lower than that of cisplatin (range from 6.3 to 3.1 μM against 9.1 μM for cisplatin). Furthermore, complexes $\mathbf{2}^{+}$, $\mathbf{4}^{+}$, $\mathbf{5}^{+}$ and $\mathbf{6}^{+}$ are able to circumvent cisplatin cellular resistance.

Introduction

Copper plays an important role in biological systems, as do many other metals. It is involved in many primordial processes such as dioxygen transport, oxidation processes, signalling, *etc*. Recently, copper has also been shown to be a cofactor essential for the tumour angiogenesis processes, in contrast to other transition metals.[1,2] High serum and tissue levels of copper were, for instance, found in many types of human cancer (breast, prostate, colon, lung, and brain).[3,4] Furthermore, patients with drug-resistant breast, colon carcinoma or lung cancer showed higher serum copper contents than patients whose tumors respond to treatment.[5] These essential observations open new prospects in anticancer strategies. For example it has been recently suggested that the copper level could be used as a marker of drug resistance.[5] On the other hand, drugs harbouring a biologically relevant metal, such as copper, were proposed to be more effective and less toxic.[2,6] They could thus represent a valuable and cheaper alternative to cisplatin ([*cis*-diamminedichloridoplatinum(II)]), which is so far the most used anti-cancer metallodrug,[7] in spite of severe side-effects and cellular resistance.[8] For example, cisplatin-based chemotherapy is the first-line therapy for metastatic bladder cancer with a response rate of approximately 50%.[9] For patients ineligible for cisplatin, there is a continued need to identify new and more effective drugs.

It has been known for decades that copper complexes could cleave DNA efficiently *in vitro* (Fig. 1). In most of the cases they are active only under specific conditions and DNA cleavage is

[a]*Département de Chimie Moléculaire, Chimie Inorganique Redox Biomimétique (CIRE), UMR CNRS 5250, Université J. Fourier, B.P. 53, 38041 Grenoble cedex 9, France. E-mail: Fabrice.Thomas@ujf-grenoble.fr; Fax: +33 476 514 836; Tel: +33 476 514 373*

[b]*AGing Imaging Modeling, FRE 3405, Université Joseph Fourier, CNRS, EPHE, UPMF, 38706 La Tronche cedex, France*

†Electronic supplementary information (ESI) available. CCDC 795941, 795943 and 795944. For ESI and crystallographic data in CIF or other electronic format see DOI: 10.1039/c3dt32659d

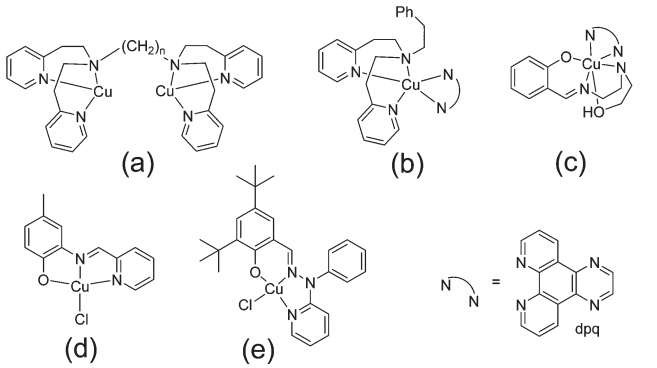

Fig. 1 Copper complexes exhibiting a DNA cleavage activity: (a) in the presence of a reductant or H_2O_2;[11] (b) upon irradiation,[13] (c, d, e) without an external agent.[17,22,23]

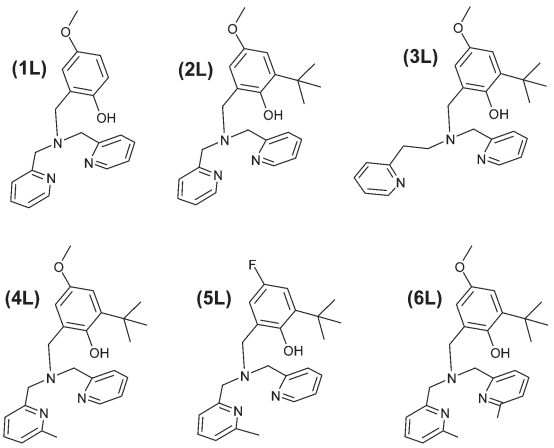

Fig. 2 Formula of the ligands used in this study.

promoted by reactive oxygen species (ROS).[10–14] As a result, the nuclease activity is observed upon the addition of a reductant (mercaptan) or a co-oxidant (such as H_2O_2) to the copper(II) complex.[11,12] A prototypical example is the dicopper(II) complex of the bis(bipyridylamine) ligand shown in Fig. 1a. The mercaptan reduces the copper(II) center into copper(I), which then reacts with dioxygen to form reduced ROS (O_2^{2-}, $O_2^{\cdot -}$ and/or $OH^{\cdot}$) responsible for DNA cleavage. The addition of H_2O_2 to similar copper(II) complexes also induces DNA cleavage, but in this case metal coordination facilitates deprotonation of hydrogen peroxide, thereby dramatically enhancing its reactivity.[10] An alternative strategy to generate toxic ROS is the use of copper(II) complexes involving a photo-sensitizer such as dpq (Fig. 1). Upon irradiation the copper complex depicted in Fig. 1b[13] forms highly reactive singlet oxygen $^1O_2$, which damages DNA.[13,14]

Copper complexes that cleave DNA without the need for an external agent are more interesting for an *in cellulo* use, but they are much rarer. Their development is a subject of current interest.[15–23] The nuclease activity of copper(II) complexes in the absence of an exogenous agent results from either hydrolytic or oxidative catalysis. Neves *et al.*[15,16] and Palaniandavar *et al.*[17,18] developed several copper complexes (Fig. 1c) able to mediate hydrolytic DNA cleavage: The role of the metal ion is here to favour the nucleophilic attack at the DNA phosphates. The copper complexes of Tambjamine E and Doxycycline are rare examples of oxidative cleavage whereby the ligand itself reduces Cu(II) into Cu(I), which further reduces O_2 into reactive $O_2^{\cdot -}$.[19,20] ROS were also identified as responsible for DNA cleavage in some other cases but their origin was unclear.[21] Recently, a high DNA cleavage activity has been reported for the copper(II)-phenolate complex depicted in Fig. 1d. This complex also exhibits a significant anti-proliferative activity towards L1210 murine leukemia cancer cell line and A2780 human ovarian carcinoma cell line, with IC_{50} values similar to cisplatin (3.4–10.3 μM).[22] Its reactivity towards DNA was quite original since the proposed reactive species is a Cu(II)-phenoxyl radical formed during aerobic oxidation of the phenolate complex.[22] Similar phenoxyl radical species were proposed later by Ghosh *et al.* to account for the nuclease activity of related copper(II) and zinc(II) phenolate complexes.[23]

In this study, we investigate the coordination chemistry, the DNA cleavage activity (in the absence of an external agent) and the anti-proliferative effect against a bladder tumor cell line of a series of copper(II) complexes involving a sterically hindered (and thus pro-phenoxyl radical) phenolate group (Fig. 2). Variations in the phenolic *ortho* substituent, as well as in the alkylpyridine arms, are shown to dramatically influence both DNA cleavage and biological activity.

Results and discussion

Synthesis of the ligands and copper complexes

The ligands 1L, 2L, 4L, 5L and 6L (Fig. 2) were obtained by condensation of the appropriate phenol with bis-pyridin-2-ylmethyl-amine derivatives in the presence of formaldehyde. 3L was synthesized by reductive amination of 3-*tert*-butyl-2-hydroxy-5-methoxy-benzaldehyde in the presence of (2-pyridin-2-yl-ethyl)-pyridin-2-ylmethyl-amine; the complexes were synthesized by reacting the ligand with one molar equivalent of $Cu(ClO_4)_2{\cdot}6H_2O$ in methanol ($\mathbf{1}^{2+}$) or acetonitrile ($\mathbf{2}^{+}$–$\mathbf{5}^{+}$).

The copper complex of 1L was isolated in the presence of base in dimeric form. Brown single crystals of $\mathbf{1{\cdot}(ClO_4)_2{\cdot}(CH_3CN)_4}$ were grown by slow diffusion of diethyl ether into a methanolic solution of the complex (Table 1). The copper complexes of 2L–5L, namely $\mathbf{2}^{+}$–$\mathbf{5}^{+}$, were isolated as monomers due to the steric bulk at the *ortho* position of the phenol. We reported previously the crystal structure of $\mathbf{2{\cdot}ClO_4}$.[24] Blue crystals of $\mathbf{3{\cdot}ClO_4}$, $\mathbf{4{\cdot}ClO_4}$ and $\mathbf{5{\cdot}ClO_4}$ were grown by slow diffusion of diethyl ether into a concentrated solution of the complex in acetonitrile. Only the former two gave crystals of sufficient quality for an X-ray diffraction analysis. Attempts to crystallize the copper complex of 6L in a similar manner were unsuccessful: mixing one equivalent of ligand with the copper salt in CH_3CN affords a blue solution that quickly turns green and then colourless. It is likely that the steric demand of two α-methylpyridines decreases the copper binding constant.

Table 1 Crystallographic data for the copper complexes **1·(ClO$_4$)$_2$·(CH$_3$CN)$_4$**, **3·ClO$_4$** and **4·ClO$_4$**

	1·(ClO$_4$)$_2$·(CH$_3$CN)$_4$	**3·ClO$_4$**	**4·ClO$_4$**
Formula	$C_{48}H_{52}Cu_2N_{10}O_{12}Cl_2$	$C_{27}H_{34}CuN_4O_{10}Cl_2$	$C_{27}H_{34}CuN_4O_{10}Cl_2$
M	1158.98	709.02	709.02
Crystal system	Monoclinic	Monoclinic	Triclinic
Space group	$P121/c1$	$P121/n1$	$P\bar{1}$
a/Å	11.731(2)	15.395(3)	8.792(2)
b/Å	19.464(4)	10.905(2)	9.363(2)
c/Å	10.997(2)	18.813(4)	19.591(4)
α/°	90	90	83.90(3)
β/°	93.31(3)	90.53(3)	78.29(3)
γ/°	90	90	83.83(3)
V/Å^3	2506.6(9)	3158(1)	1564.2(5)
Z	2	4	2
T/K	150	293	293
D_c/g cm^{-3}	1.536	1.491	1.505
μ (cm^{-1})	10.28	9.21	9.30
Monochromator	Graphite	Graphite	Graphite
Wavelength	MoKα (0.71073 Å)	MoKα (0.71073 Å)	MoKα (0.71073 Å)
Reflections collected	30 584	34 696	47 781
Independent reflections (R_{int})	10 407 (0.0437)	6544 (0.0622)	9782 (0.0381)
Observed reflections	7267 [$I > 2\sigma(I)$]	4950 [$I > 2\sigma(I)$]	7148 [$I > 2\sigma(I)$]
R	0.0433	0.0564	0.0457
R_w	0.1045	0.1451	0.1081

Since unchelated copper(II) is known to be a strong oxidizer in CH$_3$CN it may slowly oxidize the phenol into a phenoxyl radical (well-known green colour), which further decomposes.[25] This assumption is confirmed by the fact that replacing CH$_3$CN by DMF prevents this phenomenon. The desired complex **6$^+$** was thus generated *in situ* in DMF for further analysis by adding one molar equivalent of Cu(ClO$_4$)$_2$·6H$_2$O to the ligand 6L. Noteworthy, **6$^+$** is mainly in its phenolate form (see ESI†) in this solvent, due to the basic character of DMF.

X-ray crystal structures of the copper complexes

The ORTEP views of **1^{2+}**, **3$^+$**, **4$^+$** are shown in Fig. 3 and 4, and selected bond lengths and angles are listed in Table 2.

In **1^{2+}** the two copper atoms have similar pentacoordinate environments that share the oxygen atoms O1 and O1* from two ligands. The geometry around the metal ion is intermediate between trigonal-bipyramidal and square-pyramidal. The

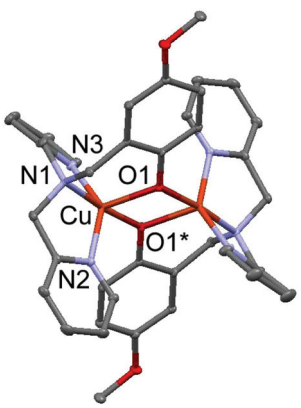

Fig. 3 X-ray crystal structures of **1^{2+}** shown with 30% thermal ellipsoids. H atoms are omitted for clarity.

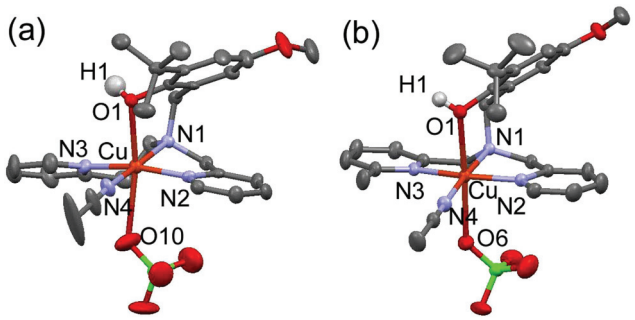

Fig. 4 X-ray crystal structures of **3$^+$** and **4$^+$** shown with 30% thermal ellipsoids. H atoms are omitted for clarity, except H1.

Table 2 Selected bond lengths (Å) and angles (°) for the copper complexes **1^{2+}**, **3$^+$** and **4$^+$**

1^{2+}		
Cu–O1 2.110(1)	Cu–O1* 1.944(1)	Cu–N1 2.026(2)
Cu–N2 2.022(2)	Cu–N3 2.000(2)	
O1–Cu–O1* 82.1(1)	O1–Cu–N1 93.4(1)	O1–Cu–N2 100.8(1)
O1–Cu–N3 117.5(1)	O1*–Cu–N1 174.5(1)	O1*–Cu–N2 101.2(1)
O1*–Cu–N3 95.5(1)	N1–Cu–N2 82.6(1)	N1–Cu–N3 84.0(1)
N2–Cu–N3 140.1(1)		
3$^+$		
Cu–O1 2.460(4)	Cu–O10 2.826(6)	Cu–N1 2.062(3)
Cu–N2 2.001(3)	Cu–N3 2.008(3)	Cu–N4 2.014(3)
O1–Cu–O10 170.7(2)	O1–Cu–N1 87.9(1)	O1–Cu–N2 92.6(1)
O1–Cu–N3 99.7(2)	O1–Cu–N4 87.4(2)	N1–Cu–N2 83.1(2)
N1–Cu–N3 93.8(2)	N1–Cu–N4 173.3(2)	N2–Cu–N3 167.3(2)
N2–Cu–N4 92.3(2)	N3–Cu–N4 91.7(2)	
4$^+$		
Cu–O1 2.444(2)	Cu–O6 2.495(2)	Cu–N1 2.013(2)
Cu–N2 2.016(2)	Cu–N3 2.066(2)	Cu–N4 1.985(2)
O1–Cu–O6 176.5(1)	O1–Cu–N1 89.5(1)	O1–Cu–N2 90.0(1)
O1–Cu–N3 95.4(1)	O1–Cu–N4 91.6(1)	N1–Cu–N2 82.9(1)
N1–Cu–N3 82.3(1)	N1–Cu–N4 175.4(1)	N2–Cu–N3 164.5(1)
N2–Cu–N4 92.7(1)	N3–Cu–N4 102.0(1)	

relative extent of the trigonal-bipyramidal distortion is indicated by an index τ representing the degree of trigonality within the structural continuum between square-planar and trigonal-bipyramidal structures.[26] The τ index calculated according to the equation $\tau = (\beta - \alpha)/60$ (where β = O1*–Cu–N1 and α = N2–Cu–N3) is 0.58. Assuming that 0 corresponds to a perfect square pyramidal geometry and 1 a perfect trigonal bipyramid, the geometry around the metal center in $\mathbf{1}^{2+}$ could be thus better described as distorted trigonal-bipyramidal. Each copper atom is coordinated to three nitrogen and two oxygen atoms: the pyridine nitrogens N2 and N3, the tertiary amino nitrogen N1 and two μ-phenolato oxygens O1, O1*. The Cu–O1 bond (2.110(1) Å) is longer than the Cu–O1* one (1.944(1) Å) and the O1–Cu–O1* angle (82.1(1)°) is significantly different from the Cu–O1–Cu one (97.9(1)°). The CuO1CuO1* unit is found to be completely flat, in contrast with butterfly shapes commonly observed in dimers of tripodal ligands involving two phenolato donors (N_2O_2 donor set).[24,27] As a consequence the intermetallic distance is longer, the Cu–Cu bond length being 3.060(1) Å.

$\mathbf{3}^{+}$ contains a copper atom within an axially elongated octahedral geometry. One tertiary amine N1 and two pyridine N2, N3 nitrogen donors from the ligand, as well as one nitrogen N4 from an exogenous acetonitrile molecule coordinate in the equatorial positions. The axial positions are occupied by two oxygen donors, one from the phenol moiety (O1) and the other (O10) from an exogenous perchlorate ion. The copper–nitrogen bond distances Cu–N1, Cu–N2, Cu–N3 and Cu–N4 are 2.062(3), 2.001(3), 2.008(3) and 2.014(3) Å respectively, whereas the axial copper–oxygen bond distances Cu–O1 and Cu–O10 are found to be much longer, 2.460(4) and 2.826(6) Å, with a copper displaced 0.068 Å above the mean plane formed by the four nitrogen donors, toward the axial O1 atom. The large axial bonds reflect the very weak donor ability of the phenol and perchlorate ligands, and the sensitivity of the d^9 electronic configuration to Jahn–Teller distortion. Interestingly, a hydrogen bond exists between the phenol hydrogen H1 and the oxygen of one perchlorate molecule (O1–O4 bond distance of 2.76 Å). It is noticeable that the two copper–pyridine nitrogen bond distances Cu–N2 and Cu–N3 were found to be short, nearly equivalent in the previously described complex $\mathbf{2}^{+}$ (1.974(3) and 1.983(3) Å). The longer Cu–N2 and Cu–N3 bond distances observed in the case of $\mathbf{3}^{+}$ (2.001(3) and 2.008(3) Å) likely originate from the formation of an in-plane 6-membered rather than 5-membered coordination ring.[28] The two pyridine nitrogen atoms N2 and N3 are located 0.153 and 0.138 Å below the mean plane defined by the N1,N2,N3,N4 atoms, whereas the tertiary amine and acetonitrile nitrogens are located 0.149 and 0.142 Å above this mean plane, with an angle between the two N1–Cu–N3 and N2–Cu–N4 planes of 12.8°. In the case of $\mathbf{2}^{+}$, we have reported that the mean displacement of the nitrogens with respect to the four nitrogens plane was only 0.055 Å, whereas the angle between the two opposite N–Cu–N planes was 10.2°. Therefore, an increase in the length of the linker between the tertiary amine nitrogen and one pyridine results in a marked tetrahedral distortion of the copper ion.

The geometry of $\mathbf{4}^{+}$ is roughly similar to that observed for $\mathbf{3}^{+}$, with the metal ion lying within an axially elongated octahedral geometry. The copper atom is coordinated in the equatorial plane by one tertiary nitrogen N1, two pyridine nitrogens N2 and N3 and one acetonitrile nitrogen N4. The phenol oxygen O1 and one perchlorate oxygen O5 bind weakly in axial position with Cu–O1 and Cu–O5 bond distances of 2.444(2) and 2.495(2) Å respectively. The copper–nitrogen bond distances Cu–N1, Cu–N2, Cu–N3 and Cu–N4 are 2.013(2), 2.016(2), 2.066(2) and 1.985(2) Å respectively. It is noteworthy that the Cu–N3 bond is the weakest Cu–N bond in the series, as a result of the incorporation of a steric bulk at the α-position of the pyridine.[29] The angle between the two planes defined by the N1–Cu–N3 and N2–Cu–N4 atoms is rather small (only 4.8°), in contrast with $\mathbf{2}^{+}$ and $\mathbf{3}^{+}$. The weakening of one of the pyridine–metal bonds thus favours an almost square planar equatorial geometry around the copper ion.

EPR properties of the complexes

The EPR spectra of the copper(II) complexes were recorded in a water–DMF (90 : 10) mixture due to their low solubility in pure water. The 100 K EPR spectra recorded at pH 7.3 are shown in Fig. 5. They all consist of an (S = 1/2) signal with copper hyperfine structure, which is typical of mononuclear complexes. This result is not surprising for complexes $\mathbf{2}^{+}$–$\mathbf{5}^{+}$ since they were isolated as monomers in the solid state. Regarding $\mathbf{1}^{2+}$, a water or DMF molecule likely acts as a fifth ligand, thereby replacing one μ-phenolate moiety in the copper coordination sphere (Scheme 1).

In order to confirm this hypothesis we recorded the EPR spectrum of $\mathbf{1}^{2+}$ in the less coordinating solvent CH_3CN. No signal could be evidenced at 100 K, showing that $\mathbf{1}^{2+}$ cannot be described as two isolated (S = 1/2) spins. Clearly, the two copper(II) ions are magnetically exchange coupled. This result

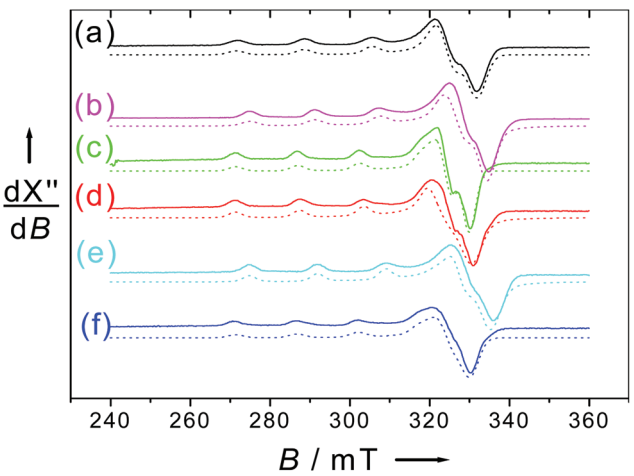

Fig. 5 X-band EPR spectra of 0.5 mM solutions of (a) $\mathbf{1}^{2+}$, (b) $\mathbf{2}^{+}$, (c) $\mathbf{3}^{+}$, (d) $\mathbf{4}^{+}$, (e) $\mathbf{5}^{+}$ and (f) $\mathbf{6}^{+}$ in a water–DMF 90 : 10 mixture at pH 7.3 ([Tris] = 0.05 M, [NaCl] = 0.02 M). Solid lines represent experimental spectra, and dotted lines represent simulations using parameters given in the text. T = 100 K, microwave frequency 9.34 GHz (a, c, d, f) or 9.44 GHz (b, e), power 10 mW, modulation frequency 100 kHz, amplitude 0.3 mT.

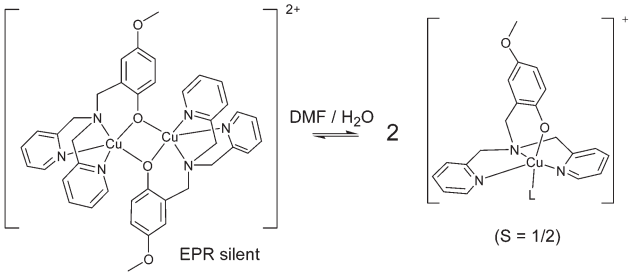

Scheme 1 Dissociation of the dimer $\mathbf{1}^{2+}$ in aqueous solution (L = H_2O or DMF).

Table 3 Spin Hamiltonian parameters for mononuclear copper complexes[a]

Complex	g values g_{xx}, g_{xy}, g_{zz}	A_{Cu} (mT) A_{xx}, A_{yy}, A_{zz}
$\mathbf{1}^{2+}$	2.053, 2.053, 2.248	1.0, 1.0, 17.0
$\mathbf{2}^{+}$	2.057, 2.057, 2.253	1.5, 1.5, 16.3
$\mathbf{3}^{+}$	2.055, 2.055, 2.262	1.0, 1.0, 15.5
$\mathbf{4}^{+}$	2.055, 2.055, 2.255	1.5, 1.5, 16.1
$\mathbf{5}^{+}$	2.057, 2.057, 2.245	1.5, 1.5, 17.1
$\mathbf{6}^{+}$	2.053, 2.053, 2.265	1.0, 1.0, 15.3

[a] Concentration of the complexes: 0.5 mM; medium: water + 0.05 M Tris HCl buffer pH 7.5 + 10% (vol) DMF. T = 100 K.

is not surprising if one considers $\mathbf{1}^{2+}$ as dimer. Both the short intermetallic distance and the favorable orbital overlap lead to a significant magnetic interaction between the paramagnetic (S = 1/2) metal ions. The resulting system is diamagnetic or paramagnetic (S = 1).

From the simulation of the spectra in the water–DMF (90 : 10) mixture, we obtained the spin Hamiltonian parameters listed in Table 3. They are consistent with an essentially square pyramidal geometry for the copper center. Interestingly, slight differences of g_{zz} are observed in the complexes, reflecting distortions in the metal ion geometry within the series.

Electronic spectra of the complexes

The electronic spectra of the copper complexes were recorded in a water–DMF (90 : 10) mixture at pH 7.3 (Fig. 6, Table 4). The electronic spectrum of $\mathbf{1}^{2+}$ displays two main transitions at 470 nm (ε = 880 M^{-1} cm^{-1}) and 690 nm (ε = 340 M^{-1} cm^{-1}). Based on its low intensity the latter is attributed to d–d transitions. The higher energy band, which is absent in the spectrum of the free ligand, arises from a phenolate-to-copper CT transition. The spectra of $\mathbf{2}^{+}$, $\mathbf{3}^{+}$ and $\mathbf{4}^{+}$ exhibit similar shapes, with a dominating band at *ca.* 500 nm and a less intense shoulder above 700 nm (Table 4). Comparison with the literature data[24] shows that the former band arises from a phenolate-to-copper(II) charge transfer (CT), while the latter is assigned to d–d transitions. For copper(II) complexes of tripodal ligands it has been proposed that the shape of the d–d band, and especially the presence of a high or low-energy shoulder, reflects the geometry of the metal ion.[26] A high-energy shoulder is indicative of trigonal bipyramidal geometry,

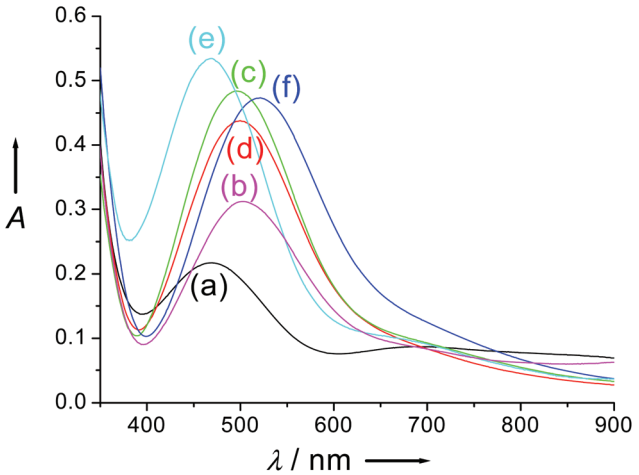

Fig. 6 UV-Vis spectra of 0.5 mM solutions (except (e): 0.25 mM) of the complexes in a water–DMF 90 : 10 mixture at pH 7.3 ([Tris] = 0.05 M, [NaCl] = 0.02 M): (a) $\mathbf{1}^{2+}$, (b) $\mathbf{2}^{+}$, (c) $\mathbf{3}^{+}$, (d) $\mathbf{4}^{+}$, (e) $\mathbf{5}^{+}$, (f) $\mathbf{6}^{+}$. T = 298 K, l = 1.000 cm.

Table 4 UV-Vis properties of the complexes at pH 7.3 in water–DMF (90 : 10) and thermodynamic constants

Complex	λ_{max}/nm (ε/M^{-1} cm^{-1})[a]	pK_a (phenol)[c]	K_b[e] (M^{-1})
$\mathbf{1}^{2+}$	470 (880), 690br (340)	—[d]	7770 ± 1500
$\mathbf{2}^{+}$	501 (620)/501 (890)[b]	6.98 ± 0.02	2580 ± 300
$\mathbf{3}^{+}$	496 (970)	5.80 ± 0.03	1940 ± 550
$\mathbf{4}^{+}$	500 (880)	5.49 ± 0.02	—[f]
$\mathbf{5}^{+}$	468 (1070)	—[d]	—[f]
$\mathbf{6}^{+}$	521 (950)	4.44 ± 0.04	—[g]

[a] 0.05 M Tris buffer + 0.02 M NaCl at 298 K. [b] The first value at pH 7.3 in 0.05 M Tris + 0.02 M NaCl, and the second value at pH 9 in $NaClO_4$ 0.1 M medium. [c] 0.1 M $NaClO_4$. [d] Precipitation is observed at neutral pH in the presence of 0.1 M $NaClO_4$. [e] Binding constant for CT DNA in a 0.05 M Tris buffer + 0.02 M NaCl at 298 K. [f] The spectral variations are too small to determine a binding constant. [g] Significant DNA digestion occurs during titration.

whereas a low-energy shoulder is rather indicative of square pyramidal geometry. The significant overlap between the CT transitions and the d–d bands precludes such a detailed analysis. Nevertheless the observed NIR-tailoring, together with the EPR results, is fully consistent with a square pyramidal geometry of the copper ion. This assumption is further confirmed by the close similarity between the spectra of $\mathbf{2}^{+}$, $\mathbf{3}^{+}$, $\mathbf{4}^{+}$, $\mathbf{5}^{+}$, $\mathbf{6}^{+}$ and some structurally characterized copper(II) phenolate complexes where the metal ion lies in a square pyramidal geometry.[28–32] On the basis of the reported ε values for phenolate-to-copper CT (*ca.* 1000 M^{-1} cm^{-1}) for complexes having the same geometry[24,28,29] it is reasonable to assume that $\mathbf{3}^{+}$ and $\mathbf{4}^{+}$ exist almost exclusively in their deprotonated phenolate form at pH 7.3 (in other words, their phenol's pK_a is lower than 6) (Scheme 2).

Of interest is the lower intensity of the LMCT band of $\mathbf{2}^{+}$, which suggests that the phenol's pK_a is much higher for this compound (see below). We previously reported the spectrum of $\mathbf{2}^{+}$ in its deprotonated phenolate form in CH_3CN, which is characterized by an absorption maximum at *ca.* 530 nm.[29] The shift of 30 nm resulting from the change of solvent

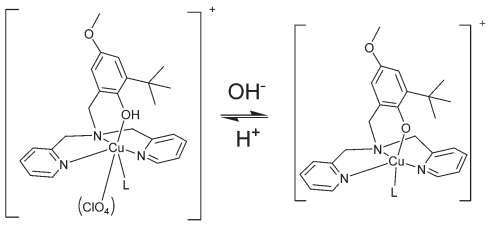

Scheme 2 Acid–base equilibrium for $\mathbf{2}^{+}$ in H_2O–DMF solution (L = H_2O or DMF).

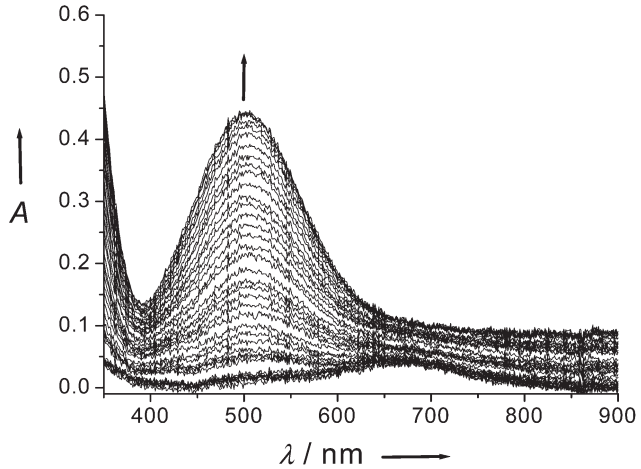

Fig. 7 Evolution of the UV-Vis spectra as a function of pH of a 0.5 mM solution of $\mathbf{2}^{+}$ in a water–DMF 90 : 10 mixture ([$NaClO_4$] = 0.1 M): T = 298 K, l = 1.000 cm. Arrows indicate spectral changes upon an increase of the pH from 3.54 to 8.84.

confirms that the coordinating CH_3CN molecule (observed in the X-ray crystal structure) is substituted in the water–DMF medium (Scheme 2). The spectrum of $\mathbf{5}^{+}$ resembles that of $\mathbf{4}^{+}$, although the CT band is blue-shifted by 32 nm. This behaviour is easily explained by the weaker electron-donating ability of the fluorine group, when compared to the methoxy substituent.[24] More surprising, the phenolate-to-copper CT is observed at 521 nm for $\mathbf{6}^{+}$ while it appeared at 500 nm for $\mathbf{4}^{+}$, which exhibits a similar *para* phenolate substituent. Such a trend was also reported by Shimazaki *et al.* for related copper complexes.[29] A possible explanation is a difference in the geometry of the phenolate complexes, which affects the strength of the Cu–O bond.[29]

We investigated the pH-dependence of the UV-Vis spectra (Fig. 7) in the pH range 3.5–9 in a water–DMF (90 : 10) mixture (+0.1 M $NaClO_4$). Except for $\mathbf{1}^{2+}$ and $\mathbf{5}^{+}$, which were found to be insufficiently soluble at neutral pH in this medium, we observed perfect agreement between the spectra at pH 7.3 in the 0.1 M $NaClO_4$ and the 0.05 M Tris media. This shows that the buffer or supporting electrolyte does not interfere with complexes $\mathbf{2}^{+}$, $\mathbf{3}^{+}$, $\mathbf{4}^{+}$ and $\mathbf{6}^{+}$. For these complexes an increase in pH from 7 to 9 does not induce a significant shift of λ_{max}, indicating that the pK_a of the coordinated water molecule is relatively high (>10) or DMF binds instead. In contrast, a decrease in pH down to 3.5 results in the disappearance of the phenolate-to-copper CT band, consistent with protonation of the phenolate moiety (Scheme 2). The titration data were refined with SPECFIT software in order to extract the phenol's pK_as. The computed pK_as are found to be 6.98 ± 0.02, 5.80 ± 0.03, 5.49 ± 0.02 and 4.44 ± 0.04 for $\mathbf{2}^{+}$, $\mathbf{3}^{+}$, $\mathbf{4}^{+}$ and $\mathbf{6}^{+}$ respectively. Noteworthy, the pK_a value measured for $\mathbf{2}^{+}$ is close to that reported for the axial tyrosine in the copper active site of Galactose Oxidase (*ca.* 8)[30] and structurally characterized copper complexes involving axial phenol/phenolates.[31]

The trend of pK_a $\mathbf{2}^{+}$ > $\mathbf{4}^{+}$ > $\mathbf{6}^{+}$ indicates that substitution of the pyridines by methylpyridines stabilizes the phenolate forms. This feature likely arises from geometrical rearrangements associated with deprotonation.[32] Indeed, phenols are weak donors that systematically coordinate the copper in axial position. Exhaustive structural characterizations on copper(II)-phenolate complexes of N_3O tripodal ligands related to $\mathbf{2}^{+}$ (*i.e.* involving exclusively two pyridin-2-ylmethyl N-donors) revealed that the phenolate moiety usually coordinates in axial position.[24,33,34] On the other hand, Shimazaki *et al.* investigated copper(II)-phenolate complexes of N_3O tripodal ligands involving one or two 6-methylpyridin-2-ylmethyl N-donors.[29] They reported that the phenolate group occupies systematically the equatorial position. This behaviour is ascribed to the steric hindrance of the methyl group, which forces the methylpyridine to coordinate in an axial position. A noticeable lowering of pK_a is also observed on increasing the size of the chelate ring involving the pyridine nitrogen, as reflected by the difference in pK_a between $\mathbf{2}^{+}$ and $\mathbf{3}^{+}$. Previously, it was found that the nature of the chelate rings could influence the positioning of the phenolate (the steric constraint at the copper center differs on replacing the five-membered chelate rings by six-membered ones), but the phenomenon is less clear. For example the copper(II) complex of the 4-nitro-2-{[(2-pyridin-2-yl-ethyl)-pyridin-2-ylmethyl-amino]-methyl}-phenolate ligand exhibits an axially bound phenolate,[33] in contrast with the complex of the 2,4-di-*tert*-butyl-6-{*N*,*N*-bis[2-(2-pyrid-2-ylethyl]-amino]-methyl}-phenolate[28] and 4-nitro-2-{*N*,*N*-bis[2-(2-pyrid-2-ylethyl]amino]-methyl}-phenolate ligands,[35] where the phenolate coordinates in equatorial position. We will therefore limit our discussion to $\mathbf{2}^{+}$, $\mathbf{4}^{+}$ and $\mathbf{6}^{+}$ and interpret the lower pK_as of $\mathbf{4}^{+}$ and $\mathbf{6}^{+}$, when compared to $\mathbf{2}^{+}$, by a structural rearrangement induced by deprotonation of the phenol moiety.[32]

The UV-Vis spectra of the copper complexes were recorded after 10 min incubation with calf thymus DNA (concentrations up to 500 μM in mole base pairs). On increasing the DNA concentration a decrease in the intensity of the CT band is observed for $\mathbf{1}^{2+}$, $\mathbf{2}^{+}$ and $\mathbf{3}^{+}$, while very little change was observed for $\mathbf{4}^{+}$ and $\mathbf{5}^{+}$. Noteworthy, we did not observe a significant red shift of the CT band. A plot of [DNA]/($\varepsilon_a - \varepsilon_f$) (where ε_a is the apparent molar extinction coefficient at a given DNA concentration and ε_f is the molar extinction coefficient of the free complex) as a function of DNA concentration gives a straight line (Fig. 8) for $\mathbf{1}^{2+}$ and $\mathbf{2}^{+}$ from which the intrinsic binding constants K_b could be calculated (see the Experimental section). In the case of $\mathbf{3}^{+}$ the absorbance change resulting from DNA binding is smaller than that for $\mathbf{2}^{+}$ and $\mathbf{3}^{+}$;

consequently the resolution is poorer and the uncertainty higher. Based on structural similarities between $\mathbf{1}^{2+}$, $\mathbf{2}^{+}$ and $\mathbf{3}^{+}$ we assumed that the dependence of $[DNA]/(\varepsilon_a - \varepsilon_f)$ *vs.* [DNA] was linear in the latter case and treat the data accordingly. The binding constants K_b (Table 4) determined from the spectral change are 7770 ± 1500, 2580 ± 300 and 1940 ± 550 M^{-1} for $\mathbf{1}^{2+}$, $\mathbf{2}^{+}$ and $\mathbf{3}^{+}$, respectively. As expected, the K_b value of $\mathbf{1}^{2+}$ is the highest, due to the lack of steric hindrance at the *ortho* position of the phenolate group. The K_b values are lower than those of typical intercalators such as EthBr ($K_b = 1.4 \times 10^6$ M^{-1}) and partially intercalating complexes such as heteroleptic [Cu(tdp)(dipyrido-[3,2-d2′,3′-f]-quinoxaline)]$^{+}$ (9×10^5 M^{-1}).[17] They are typical of weak DNA binding interactions, as observed in the [Cu(tdp)(bipyridine)]$^{+}$ complex (K_b = 7100 M^{-1}) and derivatives[17] and very close to that recently reported for the copper complex of the [(2-pyridin-2-yl-ethyl)-pyridin-2-ylmethyl-amino]-methyl ligand (roughly 10^4).[36] The efficient nuclease $\mathbf{6}^{+}$ (see below) exhibits a dramatically different behaviour. Indeed, the spectra were found to evolve significantly with time, with a progressive decrease of the CT band. This suggests that significant DNA digestion occurs during the titration experiment, thus precluding refinement of the data to extract binding constants.

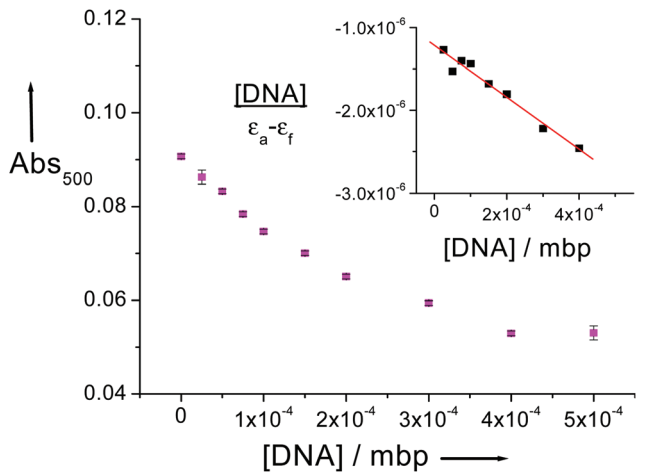

Fig. 8 Plot of the absorbance at 500 nm as a function of DNA concentration (expressed in mole base pairs) for a 0.22 mM solution of $\mathbf{2}^{+}$ in a water–DMF 90 : 10 mixture at pH 7.3 ([Tris] = 0.05 M, [NaCl] = 0.02 M). Inset: plot of $[DNA]/(\varepsilon_a - \varepsilon_f)$ as a function of the DNA concentration (ε_a is the apparent molar extinction coefficient at a given DNA concentration, and ε_f is the molar extinction coefficient of the free complex). T = 298 K, l = 1.000 cm.

Electrochemical properties of the complexes

The electrochemical behaviour of the copper complexes was investigated both at pH 7.3 (phenolate form) and 3.5 (phenol form) by cyclic voltammetry in a water–DMF (90 : 10) medium (+0.1 M $NaClO_4$). The potentials are referenced *vs.* SCE (Table 5).

At pH 7.3 all the compounds exhibit an oxidation wave in the range 0.30–0.65 V (Table 5, Fig. 9). It is found to be irreversible for both $\mathbf{1}^{2+}$ and $\mathbf{5}^{+}$ (E_p^a = 0.65 and 0.59 V respectively), while it is reversible for $\mathbf{2}^{+}$, $\mathbf{3}^{+}$, $\mathbf{4}^{+}$ and $\mathbf{6}^{+}$, *i.e.* for complexes involving an electron-rich and *o*,*p*-protected phenolate moiety ($E_{1/2}$ = 0.30, 0.32, 0.35, 0.36 V, respectively). This behaviour is strong evidence that the redox process is ligand-centered, affording phenoxyl radical species. Indeed, the potential values measured for $\mathbf{2}^{+}$, $\mathbf{3}^{+}$, $\mathbf{4}^{+}$ and $\mathbf{6}^{+}$ are very similar to those reported for $\mathbf{2}^{+}$ in CH_3CN (+0.38 V *vs.* SCE)[24] and other related

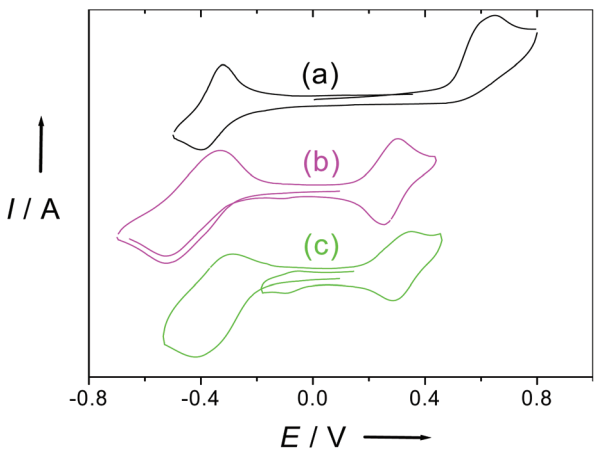

Fig. 9 Cyclic voltammetry curves of 0.5 mM solutions of the phenolate complexes in a water–DMF 90 : 10 mixture at pH 7.3: (a) $\mathbf{1}^{2+}$ in 0.05 M Tris containing 0.02 M NaCl, (b) $\mathbf{2}^{+}$ and (c) $\mathbf{3}^{+}$ in 0.1 M $NaClO_4$. Scan rate = 0.1 V s^{-1}. Potentials are given *vs.* the SCE reference.

Table 5 Electrochemical properties of the complexes[a]

	pH = 3.5		pH = 7.3[a]	
Complexes	Red[b]	Ox[c]	Red[b]	Ox
$\mathbf{1}^{2+}$	−0.35; −0.31	0.85	−0.40; −0.32[d]	E_p^a = 0.65[c,d]
$\mathbf{2}^{+}$	−0.35; −0.31	0.64	−0.56; −0.24	$E_{1/2}^1$ = 0.30; $E_p^{a,2}$ = 0.65
$\mathbf{3}^{+}$	−0.20; −0.10	0.58	−0.42; −0.29	$E_{1/2}^1$ = 0.32; $E_p^{a,2}$ = 0.57
$\mathbf{4}^{+}$	−0.22; −0.14	—[e]	−0.48; −0.24	$E_{1/2}^1$ = 0.35; $E_p^{a,2}$ = 0.63
$\mathbf{5}^{+}$	−0.23; −0.12	0.64	−0.35; −0.17[d]	$E_p^{a,1}$ = 0.59[c,d]
$\mathbf{6}^{+}$	−0.06; 0.22	0.53	−0.35; −0.16	$E_{1/2}^1$ = 0.36; $E_p^{a,2}$ = 0.56

[a] In water–DMF (90 : 10) + 0.1 M $NaClO_4$ at 298 K, except 1 and 5 at high pH. All potentials are given *vs.* the SCE reference. [b] E_p^c and E_p^a are given. [c] Irreversible processes, E_p^a is given. [d] In water–DMF (90 : 10) medium containing [Tris] = 0.05 M, [NaCl] = 0.02 M at pH 7.3 due to the low solubility of the complexes in the water–DMF (90 : 10) + 0.1 M $NaClO_4$ mixture at neutral pH. [e] Ill-defined wave.

complexes for which the copper(II)-phenoxyl radical form was electrogenerated and unambiguously identified by spectroscopy. A slight increase in oxidation potential is observed upon substitution of the pyridines by methylpyridines. The decreased N-donating ability of the methylpyridine thus destabilizes the radical form, as previously observed by Shimazaki *et al.*[29] When scanning towards the negative region of potentials a metal-centered reduction peak E_p^c is observed in the potential range −0.35 to −0.56 V (Table 5). An enhancement of the anodic peak current was observed in the reverse scan of $\mathbf{1}^{2+}$ and $\mathbf{2}^{+}$,[37] suggesting that the electron transfer involves adsorbed copper(I)-phenolate material at nearly the same potential as the "normal" electron transfer.[38] As shown in Table 4 the cathodic wave shifts to positive potentials in the order $\mathbf{2}^{+} < \mathbf{4}^{+} < \mathbf{6}^{+}$. The electron density of the copper center thus decreases with an increase in the number of methylpyridine groups in the ligand.[39] A similar anodic shift of the reduction wave is observed on going from $\mathbf{2}^{+}$ to $\mathbf{3}^{+}$ (substitution of one pyridylmethyl by a longer pyridylethyl arm). The influence of the ligand arm's length on the Cu(II)/Cu(I) redox potential in copper(II) tris(pyridyl)alkylamine complexes has been investigated recently.[40] In this case the difference in oxidation potential originates from structural rather than electronic effects: Cu(II) favours five-membered coordination rings; therefore compounds containing longer arms are stabilized in lower oxidation states and the Cu(II)/Cu(I) redox couple increases. Finally, the trend of E_p^c **4** < **5** very likely reflects the lower electron-donating ability of the fluorine substituent, which decreases the electron density at the metal.

At pH 3.5 the six compounds exhibit an irreversible oxidation wave above 0.53 V assigned to the oxidation of the phenol moiety. It is well known that oxidation of phenols occurs at potentials well above those required for oxidation of the corresponding phenolates into phenoxyl radicals.[41] The metal-centered reduction wave is observed within the potential range −0.35 to +0.32 V. Again, an abnormally high I_p^a/I_p^c ratio is observed, suggesting that the reduced complexes easily adsorb at the surface of the electrode. Interestingly, low E_p^c values were observed for $\mathbf{1}^{2+}$ and $\mathbf{2}^{+}$ (−0.31 V), while intermediate values were measured for $\mathbf{3}^{+}$, $\mathbf{4}^{+}$ and $\mathbf{5}^{+}$ (−0.20, −0.22, −0.23 respectively), and a relatively high potential (−0.06 V) was obtained for $\mathbf{6}^{+}$. This trend follows that observed for the phenolate compounds (see above) and thus will not be commented on further.

Nuclease activity of the complexes

The ability of the copper(II) complexes to cleave DNA has been investigated by gel electrophoresis using *ϕ*X174 RF1 supercoiled DNA in phosphate buffer (10 mM, pH 7.2 or 8.2 with 10% DMF). Cleavage was evidenced by monitoring the conversion of the covalently closed circular supercoiled plasmid DNA form (SC) into the nicked circular form (NC, single strand breakage) and then to the linear form (L, double strand breakage).

The nuclease activity of the complexes was first investigated at pH 7.2 and 8.2 using a constant complex concentration of

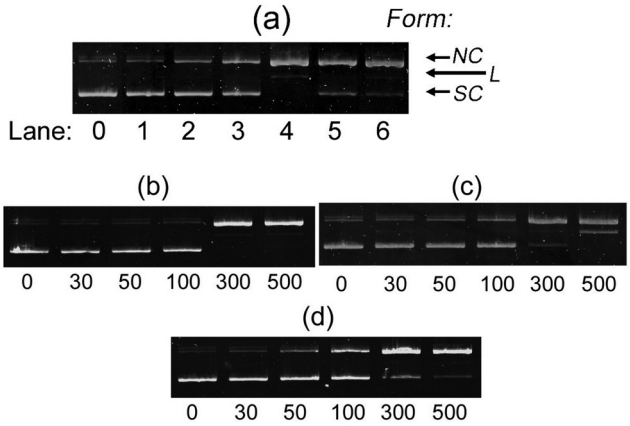

Fig. 10 Agarose gel electrophoresis patterns of the cleavage reaction of *ϕ*X174 supercoiled DNA (20 μM base pairs) mediated by the copper complexes in a phosphate buffer 10 mM, pH 7.2 (+10% DMF) at 37 °C for 1 h. Abbreviations: NC: nicked circular, L: Linear, SC: supercoiled. (a) Complex concentration = 300 μM (constant); lane 0 is the DNA control without the copper complexes; lane 1, complex $\mathbf{1}^{2+}$; lane 2, complex $\mathbf{2}^{+}$; lane 3, complex $\mathbf{3}^{+}$; lane 4, complex $\mathbf{4}^{+}$; lane 5, complex $\mathbf{5}^{+}$; lane 6, complex $\mathbf{6}^{+}$. (b, c, d): Dose dependent activity (complex concentrations are indicated in μM): (b), $\mathbf{4}^{+}$; (c), $\mathbf{5}^{+}$; and (d), $\mathbf{6}^{+}$.

300 μM. The reaction was conducted on *ϕ*X174 DNA (20 μM, in base pairs) in phosphate buffer for 1 h at 37 °C (Fig. 10a).

In the absence of complex, DNA was found to be mainly in the supercoiled form (82%) both at pH 7.2 (Fig. 10a, lane 0) and 8.2. Cleavage efficiency of the complexes was next evaluated by subtracting this starting percentage of DNA in SC form. In the presence of 300 μM of $\mathbf{1}^{2+}$, no significant change in the proportion of the SC and cleaved forms of DNA was observed (lane 1), indicating that this complex is not an efficient nuclease.

Complexes $\mathbf{2}^{+}$ and $\mathbf{3}^{+}$ were found to exhibit a moderate DNA cleavage activity, as judged by the appearance of the nicked circular form in 15 and 22% ratio, respectively, at pH = 7.2 (lanes 2 and 3, respectively). Similar moderate activities were reported for copper(II) complexes of bis(pyridyl)alkylamine ligands that do not involve an intercalating moiety.[42–44] The better activity of $\mathbf{2}^{+}$ and $\mathbf{3}^{+}$, when compared to $\mathbf{1}^{2+}$, suggests that a hydrophobic *tert*-butyl substituent in *ortho* position of the phenol enhances the nuclease activity. Since *tert*-butyl groups are expected to increase the steric protection and thus perturb the access to the metal center, the enhanced activity may result from either electronic effects, stronger hydrophobic interactions of the compound with DNA and/or differences in the complex geometry. Finally, we investigated the nuclease activity of these compounds at pH 8.2 since **2** was found to exist as a mixture of phenol and phenolate forms at physiological pH. The extent of DNA damage was found to be essentially the same within the error margin at both pH (data not shown). Interestingly, the cleavage activity of a copper(II) complex of a tripodal N_3O ligand involving a 2-hydroxy-5-methyl-benzaldehyde moiety was recently investigated by Neves *et al.* In contrast with our results they did not detect nuclease activity at pH 7, but observed significant DNA cleavage at pH 8.[16] It has to be emphasized that there are also some examples in the

literature of a drop in cleavage activity that results from an increase in pH.[45]

Complexes involving methylpyridines exhibit a remarkable nuclease activity: in the case of $\mathbf{4}^+$ total disappearance of the SC form was observed at pH 7.2 (lane 4) to the detriment of the formation of 94% of NC and 6% of L forms. Thus $\mathbf{4}^+$ promotes both single strand and double strand DNA cleavage without the need for external agents. For comparison, the recently described copper nuclease $[Cu(tdp)(dpq)]^+$ promotes only single strand cleavage under comparable conditions,[17] while the copper(II)-xylylguanidine TACN complex exhibits a similar activity.[46] The nuclease activity of $\mathbf{4}^+$ is slightly lower than that reported for the heteroleptic complex [Cu(Phen)(maltol)]$^+$ [47] and other complexes involving intercalating groups.[18,45] Complexes $\mathbf{5}^+$ and $\mathbf{6}^+$ exhibit a slightly lower activity (lanes 5 and 6 respectively) at 300 μM since the SC DNA form was not fully converted to the NC form (17% and 29% of the SC form remains for 83% and 71% of the NC form produced, for compounds $\mathbf{5}^+$ and $\mathbf{6}^+$, respectively), while double strand cleavage (L form) was not observed. For the latter compounds a moderate enhancement of the nuclease activity was observed at higher pH (full digestion), thus supporting a hydrolytic pathway (data not shown).

For the most active compounds $\mathbf{4}^+$, $\mathbf{5}^+$ and $\mathbf{6}^+$ we investigated the dependence of the DNA cleavage on both the concentration of the copper complexes (Fig. 10b–d) and the reaction time at a given complex concentration (300 μM, Fig. 11a–c). Not surprisingly, the higher the concentration, the greater the yield in cleavage product (Fig. 10b–d). For $\mathbf{5}^+$ and $\mathbf{6}^+$ the NC form could be detected for complex concentrations within the 30–50 μM range, while >90% cleavage is observed in the 300–500 μM range. There is a progressive increase of the reaction yield over a wide concentration range for $\mathbf{5}^+$ and $\mathbf{6}^+$, as shown in Fig. 10b–d. In contrast, $\mathbf{4}^+$ exhibits a dramatic enhancement of cleavage activity from 100 μM (no significant activity) to 300 μM (full digestion of the SC form). Such a dose-dependent drop in activity is rather uncommon, but it has been recently reported for the copper(II) complex of a bis(pyridyl)alkyl-acridine conjugate.[48]

For $\mathbf{4}^+$, $\mathbf{5}^+$ and $\mathbf{6}^+$ 50% cleavage of the SC form is observed for concentrations of 120 ± 50 μM. It is noteworthy that

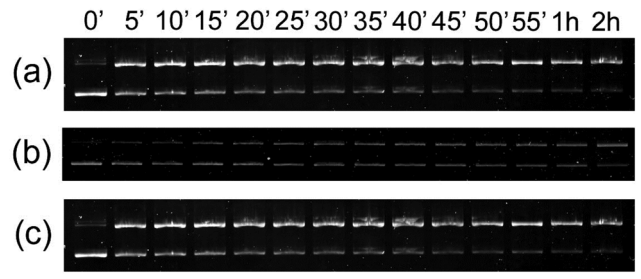

Fig. 11 Agarose gel electrophoresis patterns of supercoiled ϕX174 DNA (20 μM base pairs) incubated for different times at 37 °C with 300 μM of the copper complexes in a phosphate buffer 10 mM pH 7.2 (+10% DMF): (a) $\mathbf{4}^+$, (b) $\mathbf{5}^+$, (c) $\mathbf{6}^+$.

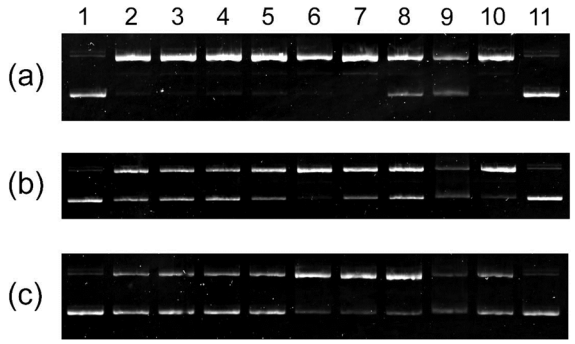

Fig. 12 Agarose gel electrophoresis patterns of supercoiled ϕX174 DNA (20 μM base pairs) incubated with the copper complexes (300 μM; excepted in lane 1) in a phosphate buffer 10 mM pH 7.2 (+10% DMF) at 37 °C for 1 h; (a) $\mathbf{4}^+$, (b) $\mathbf{5}^+$, (c) $\mathbf{6}^+$. Lane 1, DNA control; lane 2, DNA + complex (300 μM) without scavenger; lanes 3–11, DNA + complex (300 μM) in the presence of agents: lane 3, NaN_3 (100 μM); lane 4, Superoxide Dismutase (0.5 unit); lane 5, Catalase (0.1 unit); lane 6, DMSO (2 μL); lane 7, EtOH; lane 8, mercaptoethanol (0.71 mM); lane 9, Hoechst 33258 (100 μM); lane 10, NaCl (350 μM); lane 11, EDTA (10 mM).

significant amounts of double strand breakage could be evidenced for 500 μM concentrations of $\mathbf{5}^+$ and $\mathbf{6}^+$.

Examination of the time course for the reaction (Fig. 11a–c) reveals that more than 80% of plasmid is cleaved after two hours for $\mathbf{4}^+$ and $\mathbf{6}^+$ at 300 μM. The rate constants were found to be 0.49 ± 0.05 min^{-1}, 0.09 ± 0.01 min^{-1} and 0.50 ± 0.05 min^{-1} for $\mathbf{4}^+$, $\mathbf{5}^+$ and $\mathbf{6}^+$, respectively. While $\mathbf{4}^+$ and $\mathbf{6}^+$ exhibit comparable rate constants, $\mathbf{5}^+$, which exhibits a less electron-donating fluorine substituent, was found to react much slower with DNA.

In order to get insight into the reaction mechanism we evaluated the effect of various scavengers and exogenous agents on the cleavage activity (Fig. 12). For all the complexes the cleavage is fully inhibited by the addition of EDTA (lane 11), showing that the metal ion is essential for the activity. For the three compounds neither NaN_3 (singlet oxygen scavenger), superoxide dismutase (superoxide scavenger) nor Calatase (H_2O_2 scavenger) inhibit cleavage (lanes 3, 4, 5), indicating that ROS are not responsible for the activity. DMSO and EtOH also did not affect the strand scission by $\mathbf{4}^+$ (lanes 6, 7), showing that the freely diffusible $OH^{\cdot}$ species is not responsible for the cleavage. Surprisingly, DMSO was found to enhance the cleavage activity in the case of $\mathbf{5}^+$, while both DMSO and EtOH improve cleavage by $\mathbf{6}^+$. We interpret these unexpected results by a higher solubilization of the complexes in the presence of these co-solvents.

The addition of a reductant (mercaptoethanol) in the medium enhances DNA cleavage in the case of $\mathbf{6}^+$ (lane 8). This result may be understood by considering an alternative oxidative cleavage pathway,[17,18] which is initiated by reduction of the copper(II) into copper(I). This fact is consistent with electrochemical measurements, which showed that $\mathbf{6}^+$ exhibits the highest Cu(II)/Cu(I) redox potential. Mercaptoethanol slightly inhibits the activity of $\mathbf{4}^+$, while it does not affect the cleavage by $\mathbf{5}^+$. The main cleavage pathway, thus, likely remains hydrolytic for both complexes.

In the presence of a minor groove binder (Hoechst 33258) the cleavage activity of $\mathbf{4}^+$ and $\mathbf{5}^+$ was significantly inhibited (lane 9). This experiment shows that both complexes bind to DNA in the minor groove. In addition, excess of sodium chloride does not inhibit the cleavage reaction (lane 10), which rules out a simple electrostatic interaction of copper complexes $\mathbf{4}^+$ and $\mathbf{5}^+$ with DNA.

Similarly to previous studies we performed religation assays with T4 ligase on the ϕX174 DNA plasmid after incubation (1 h) with the three most active complexes $\mathbf{4}^+$, $\mathbf{5}^+$, $\mathbf{6}^+$ (300 μM) or restriction nuclease Xho I (blank).[22] For complexes $\mathbf{4}^+$, $\mathbf{5}^+$, $\mathbf{6}^+$ the initial band corresponding to the NC form of DNA is still present after religation, which would at first glance suggest an oxidative rather than hydrolytic cleavage. Nevertheless, the latter results should be used with special care since DNA hydrolysis was also assumed to be responsible for other DNA damage which could not be enzymatically religated. For instance hydrolytic cleavage products may not possess strictly matched ends suitable for religation.[50] In addition, the DNA phosphate group could remain bound to the complex after hydrolysis, and thus is inaccessible for the ligase.[15] Because the relevance of the latter experiment is not particularly strong, we still entertain the hydrolytic mechanism as the most serious option.

Anti-proliferative activity against bladder tumor cells

Some anticancer agents approved for clinical uses trigger cell death by damaging DNA. For example, platinum-containing drugs cause crosslinking of DNA,[51] Melphalan and Chlorambucil are alkylating agents[52,53] while Bleomycin acts by producing single-strand and double-strands breaks in DNA.[54] Since our molecules induced DNA cleavage, we have carried out *in vitro* assays to evaluate the cytotoxic and anti-proliferative effects of the complexes $\mathbf{1}^{2+}$–$\mathbf{6}^+$.

In order to identify more potent and safe molecules for the treatment of bladder cancer, the biological activity of our copper complexes was studied on the RT112 cell line, derived from a human bladder tumor. Cells were incubated with various concentrations of the complexes $\mathbf{1}^{2+}$–$\mathbf{6}^+$ and their proliferation was monitored by a MTT assay.[55] Our results indicate that it was necessary to treat cells for at least 48 h to observe a massive cell death. The anti-proliferative activities of tested compounds after 48 h of treatment, expressed as IC_{50} values (the concentration resulting in 50% loss of cell viability relative to untreated cells), are summarized in Table 6. Cisplatin, which is currently used in the management of advanced bladder cancer, was applied as a test referential agent.[56] Complex $\mathbf{1}^{2+}$ presented a low cytotoxic activity against RT112 cells (IC_{50} = 99.1 μM), which could be correlated to its inability to cleave DNA. For complexes $\mathbf{2}^+$ and $\mathbf{3}^+$ there seems to be no direct correlation between their moderate nuclease activity and their cytotoxicity, since IC_{50} of complex $\mathbf{3}^+$ is 6.7 times more than that of complex $\mathbf{2}^+$. Finally, complexes $\mathbf{4}^+$, $\mathbf{5}^+$ and $\mathbf{6}^+$, which have higher DNA cleavage activity, were about 1.4–2.4 times more active than cisplatin against the RT112 cell line. In order to determine if our complexes could be valuable agents to replace cisplatin in patients where cisplatin therapy failed due to chemoresistance, the four more active complexes $\mathbf{2}^+$, $\mathbf{4}^+$, $\mathbf{5}^+$ and $\mathbf{6}^+$ were tested on a bladder cancer cell line resistant to cisplatin (RT112-CP).[57] As shown in Table 6, RT112-CP cells are 2.6 times more resistant to cisplatin than the RT112 parental cell line. Interestingly, all four tested complexes (compounds $\mathbf{2}^+$, $\mathbf{4}^+$, $\mathbf{5}^+$ and $\mathbf{6}^+$) overcame the resistance observed with cisplatin as expressed by the resistance factors (RF),[22] which are lower for our complexes compared to cisplatin. Compared to the copper pyrimol complex (the structure shown in Fig. 1d)[22] the RF values are much lower and even close to 1 for $\mathbf{4}^+$, $\mathbf{5}^+$ and $\mathbf{6}^+$. So, these complexes have not only higher antitumour activity than cisplatin against a bladder cancer cell line, but also they are very powerful in circumventing the cellular resistance of RT112-CP cells.

Table 6 Anti-proliferative activity of the complexes[a]

	IC_{50} (μM)		
Complexes	RT112	RT112-CP	RF
Cisplatin	9.1 ± 1.2	23.8 ± 1.2	2.6
$\mathbf{1}^{2+}$	99.1 ± 5.8	ND	ND
$\mathbf{2}^+$	3.1 ± 0.2	5.5 ± 0.4	1.8
$\mathbf{3}^+$	20.8 ± 2.5	ND	ND
$\mathbf{4}^+$	6.3 ± 0.6	5.2 ± 0.4	0.8
$\mathbf{5}^+$	3.7 ± 0.2	5.0 ± 0.3	1.4
$\mathbf{6}^+$	3.9 ± 0.1	4.7 ± 0.5	1.2

[a] The concentration resulting in 50% loss of cell viability relative to untreated cells (IC_{50}) was determined from dose–response curves. Results represent the means ± SD of three independent experiments. RF is the relative ratio between IC_{50} of the cisplatin-resistant cells against IC_{50} of the sensitive cell lines. ND: not determined.

Effect of complexes on the cell cycle progression

In order to further characterize the mechanism of action of complexes $\mathbf{2}^+$, $\mathbf{4}^+$, $\mathbf{5}^+$ and $\mathbf{6}^+$, cell cycle analysis was performed to determine the effect of these molecules on cell cycle progression. RT112 cells were incubated with vehicle alone (DMSO) as the control, or with IC_{50} concentrations of complexes. After 24 or 48 h, cells in suspension in the medium and attached cells were harvested and analyzed by flow cytometry. As shown in Fig. 13A, after 24 h the majority of control cells (55%) are in G0/G1 phases, whereas the rest of the cells are approximately equally distributed between the S and G2 + M phases (26% and 19% respectively). A 24 h treatment of RT112 cells with complex $\mathbf{2}^+$ results in a significant accumulation of cells in the G0/G1 phase (73%), with a concomitant loss from the S phase (9%). This G0/G1 phase accumulation increases with incubation time, since it reaches 82% after 48 h against 70% in the control (Fig. 13B). The results obtained with the other complexes ($\mathbf{4}^+$, $\mathbf{5}^+$ and $\mathbf{6}^+$) are different. After 24 h of incubation with the IC_{50} concentration of the molecules, the G2 + M accumulation of cells increases from 19% in the control to 39% with complex $\mathbf{4}^+$, 34% with complex $\mathbf{5}^+$ and 44% with complex $\mathbf{6}^+$ (Fig. 13A). This is accompanied by a decrease of the number of cells in the remaining phases of the

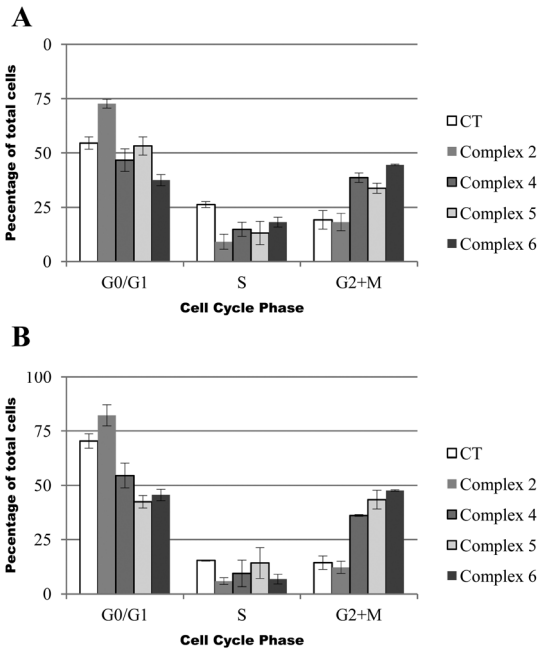

Fig. 13 Cell cycle distribution of RT112 cells treated with complexes $\mathbf{2}^+$, $\mathbf{4}^+$, $\mathbf{5}^+$ and $\mathbf{6}^+$. RT112 cells were treated with vehicle alone (Control, CT) or with the IC_{50} value of each compound for 24 h (A) or 48 h (B). Cells were then fixed, stained with PI and cell cycle was analyzed by flow cytometry. Each value is the mean ± SD of three independent determinations.

cell cycle. This G2 + M accumulation is sustained after 48 h of incubation with complex $\mathbf{4}^+$ (36% against 14% in the control) and even increased with complexes $\mathbf{5}^+$ and $\mathbf{6}^+$, which led to 43 and 48% respectively of cells in G2 + M phases (Fig. 13B).

Complexes $\mathbf{4}^+$, $\mathbf{5}^+$ and $\mathbf{6}^+$ thus clearly alter the cell cycle progression. This is most likely owing to DNA damage which results in the activation of cell cycle checkpoints in dividing cells. If cells undergo DNA damage in G2, the G2/M checkpoint is activated and stops the cell cycle to prevent cells from starting mitosis.[58,59] So, complexes $\mathbf{2}^+$, $\mathbf{4}^+$, $\mathbf{5}^+$ and $\mathbf{6}^+$ promote cell cycle arrest in G2 + M phases, which probably reflects their activity on DNA.

Conclusion

The present results point to a very simple way to dramatically enhance the nuclease activity, in the absence of an exogenous agent, of copper-phenolate complexes involving tripodal ligands: when at least one pyridine is α-methylated the yield of the reaction is significantly improved, with 75 to 95% DNA digestion after 2 hours for complex concentrations of 300 μM (*vs.* <22% for complexes involving exclusively non-methylated pyridine donors). We hypothesize that this result is correlated to the weaker N-donating ability of methylpyridines, which facilitates exchange of the coordinated exogenous ligand and modifies significantly the structure of the phenolate complex (equatorial positioning of the phenolate moiety). Noteworthy, changes in DNA binding constants do not explain directly the trend of cleavage activity in the series since $\mathbf{3}^+$ exhibits a lower affinity for DNA than $\mathbf{1}^{2+}$, although it is more active.

A hydrolytic pathway is often proposed for copper-catalyzed DNA cleavage in the absence of a reductant or oxidants. Recently, oxidative pathways were proposed to account for DNA cleavage by some copper(II) complexes involving sterically hindered phenolate or aminophenolate coordinating groups (Fig. 1d). They imply the formation of a reactive phenoxyl radical by aerobic oxidation of the coordinated phenolate. The phenoxyl/phenolate potential for the complex shown in Fig. 1d is +1.11 V *vs.* Ag/AgCl (roughly +1.07 V *vs.* SCE), *i.e.* much higher than the compounds investigated there.[22] Therefore, from a thermodynamic point of view $\mathbf{1}^{2+}$–$\mathbf{6}^+$ might form phenoxyl radicals more easily than Reedijk's complex, rendering an oxidative mechanism promoted by phenoxyl species plausible.[22] Nevertheless, large differences in chemical stabilities for the radical species (estimated *via* the I_p^a/I_p^c ratio of the phenoxyl/phenolate redox couple) were observed within our series, without any evident correlation between DNA cleavage activity and phenoxyl radical stabilities. In addition, attempts to trap a phenoxyl radical intermediate by UV-Vis spectroscopy upon reaction with DNA (phenoxyl radicals exhibit an intense π–π* transition at around 420 nm)[24] were unsuccessful. These experimental results thus argue against the involvement of a phenoxyl radical as reactive species for DNA cleavage and rather support a hydrolytic pathway. Hydrolytic DNA cleavage may be initiated by substitution of the labile coordinated solvent by a phosphate group of the DNA backbone, which is activated by the Lewis acidity of the copper ion. Methylpyridine N-donors could facilitate this activation and subsequent nucleophilic attack. A detailed investigation on the cleavage mechanism is currently under way in our laboratories.

The anti-proliferative activity of the four more active nucleases $\mathbf{2}^+$, $\mathbf{4}^+$, $\mathbf{5}^+$ and $\mathbf{6}^+$ was tested against RT112 bladder cancer cell lines. The four investigated compounds exhibit IC_{50} values lower than cisplatin (3.1–6.3 μM *vs.* 9.1 μM). They are also able to circumvent the cellular resistance of the RT112CP cell line, as reflected by RF up to three times lower for $\mathbf{2}^+$, $\mathbf{4}^+$, $\mathbf{5}^+$ and $\mathbf{6}^+$ than for cisplatin. Finally, we show here that the most active compounds alter cell cycle progression, which probably reflects their activity on DNA. Further analysis will be conducted to determine molecular alterations induced by our complexes and to understand how they could block the cell cycle at different levels.

Experimental section

Materials and methods

All chemicals were of reagent grade and were used without purification. NMR spectra were recorded on a Bruker AM 300 (^{1}H at 300 MHz) spectrometer. Chemical shifts are quoted relative to tetramethylsilane (TMS). Mass spectra were recorded on a Thermofinningen (EI/DCI) or a Bruker Esquire ESI-MS apparatus. For pK_a determinations UV/Vis spectra were recorded on

a Cary Varian 50 spectrophotometer equipped with a Hellma immersion probe (1.000 cm path length). The temperature in the cell was controlled using a Lauda M3 circulating bath and the pH was monitored using a Methrom 716 DMS Titrino apparatus. A least square fit of the titration data was realized with SPECFIT software. For UV/Vis measurements at neutral pH (buffered media) a Perkin Elmer Lambda 2 spectrophotometer was used. X-band EPR spectra were recorded on either a Bruker ESP 300E or a Bruker EMX Plus spectrometer equipped with a Bruker nitrogen flow cryostat. Spectra were simulated using Bruker SIMFONIA software. Electrochemical measurements were carried out using a CHI 620 potentiostat. Experiments were performed in a standard three-electrode cell under an argon atmosphere. A glassy carbon disc electrode (3 mm diameter) or a platinum disc electrode (1 mm diameter), which was polished with 1 mm diamond paste, was used as the working electrode. An SCE was used as the reference.

Crystal structure analysis

The collected reflections were corrected for absorption (SADABS) and solved by direct methods and refined with Olex software.[60] All non-hydrogen atoms were refined with anisotropic thermal parameters. Hydrogen atoms were generated in idealized positions, riding on the carrier atoms, with isotropic thermal parameters.

Preparation of the ligands and complexes

1L. 4-Methoxyphenol (1.24 g, 10 mmol), bis-pyridin-2-ylmethyl-amine (1.99 g, 10 mmol) and formaldehyde (0.75 ml of a 37% aqueous solution) were refluxed for 24 h in ethanol–H_2O (1 : 1, 12 ml). The reaction mixture was then extracted with dichloromethane, washed with a saturated NaCl solution and dried over Na_2SO_4. The solution was evaporated under vacuum to afford brown oil. Column chromatography on silica gel with CH_2Cl_2–methanol (10/0 to 5/5) as the eluent yielded 1L (0.67 g, 20%) as a yellow oil. ^{1}H NMR (400 MHz, $CDCl_3$): δ = 3.74 (2H, s), 3.77 (3H, s), 3.87 (4H, s), 6.64 (1H, d, ^4J = 3.0 Hz), 6.74 (1H, dd, ^3J = 8.8 Hz, ^4J = 3.0 Hz), 6.83 (1H, d, ^3J = 8.8 Hz), 7.16 (2H, dd, $^3J_1$ = 7.3 Hz, $^3J_2$ = 5.1 Hz), 7.34 (2H, d, ^3J = 7.9 Hz), 7.62 (2H, td, ^3J = 7.8 Hz, ^4J = 1.8 Hz), 8.57 (2H, d, ^3J = 4.9 Hz). 13C NMR (100 MHz, $CDCl_3$): δ = 55.9 (CH_3), 57.1 (CH_2, 59.1 (2 CH_2), 114.0 (CH), 115.9 (CH), 116.9 (CH), 122.9 (CH), 123.3 (CH), 123.4 (C), 136.8 (CH), 149.0 (CH), 151.4 (C), 152.3 (C), 158.2 (C). MS (DCI, NH_3/isobutane): *m*/*z* (%) 336.2 (100) $[M + H]^+$. M.p. 70 °C. Anal. Calcd for $C_{21}H_{25}N_3O_2$: C, 71.77; H, 7.17; N, 11.96. Found: C, 71.73; H, 6.45; N, 12.42%.

3L. 3-*tert*-Butyl-2-hydroxy-5-methoxy-benzaldehyde (208 mg, 1 mmol), (2-pyridin-2-yl-ethyl)-pyridin-2-ylmethyl-amine (213 mg, 1 mmol)[35] and glacial acetic acid (0.2 ml) were dissolved in ethanol (20 ml). After 30 min stirring, 62 mg of sodium cyanoborohydride (62 mg, 1 mmol) were slowly added (over 6 hours). The mixture was stirred for 12 hours and then neutralized with concentrated HCl (2 M). The reaction mixture was extracted with dichloromethane, washed with a saturated NaCl solution and dried over Na_2SO_4. The solution was evaporated under vacuum to afford yellow oil. Column chromatography on silica gel (ethyl acetate–pentane (1/5) yielded 3L (263 mg, 65%) as a yellow solid. ^{1}H NMR (300 MHz, $CDCl_3$): δ = 1.40 (9H, s), 2.97–3.09 (4H, m), 3.73 (3H, s), 3.83 (2H, s), 3.85 (2H, s), 7.03–7.20 (4H, m), 7.52 (1H, td, ^3J = 7.6 Hz, ^4J = 1.9 Hz), 7.57 (1H, td, ^3J = 7.6 Hz, ^4J = 1.8 Hz), 8.47 (1H, d, ^3J = 4.8 Hz), 8.52 (1H, d, ^3J = 5.9 Hz). ^{13}C NMR (75 MHz, d_6-DMSO): δ = 29.8 (3 CH_3), 35.2 (C), 35.6 (CH_2), 54.0 (CH_2), 56.0 (CH_3), 59.0 (CH_2), 59.8 (CH_2), 112.0 (CH), 113.3 (CH), 121.7 (CH), 122.6 (CH), 123.1 (C), 123.7 (CH), 123.9 (CH), 136.8 (CH), 136.9 (CH), 138.3 (C), 149.4 (CH), 149.6 (CH), 150.7 (C), 151.8 (C), 152.1 (C), 158.2 (C), 158.4 (C), 160.0 (C). MS (DCI, NH_3/isobutane): *m*/*z* (%) 406 (100) $[M + H]^+$. M.p. 70 °C. Anal. Calcd for $C_{25}H_{31}N_3O_2$: C, 74.04; H, 7.70; N, 10.36. Found: C, 73.82; H, 7.75; N, 10.31%.

4L. 2-*tert*-Butyl-4-methoxy-phenol (1.8 g, 10 mmol), (6-methyl-pyridin-2-ylmethyl)-pyridin-2-ylmethyl-amine (2.13 g, 10 mmol)[29] and formaldehyde (0.75 ml of a 37% aqueous solution) in ethanol–H_2O (4 : 6, 10 ml) were refluxed for 24 h. The reaction mixture was then extracted with dichloromethane, washed with a saturated NaCl solution and dried over Na_2SO_4. The solution was evaporated under vacuum to afford orange oil. Column chromatography on silica gel (ethyl acetate–pentane (1/1)) yielded 4L (1.82 g, 45%) as a pale pink oil. ^{1}H NMR (200 MHz, $CDCl_3$): δ = 1.45 (9H, s), 2.58 (3H, s), 3.73 (3H, s), 3.76 (2H, s), 3.83 (2H, s), 3.85 (2H, s), 6.49 (1H, d, ^4J = 3.0 Hz), 6.80 (1H, d, ^4J = 3.0 Hz), 7.00 (2H, d, ^3J = 7.5 Hz), 7.00–7.16 (2H, m), 7.38 (2H, d, ^3J = 7.8 Hz), 7.50 (1H, t, ^3J = 7.54 Hz), 7.61 (1H, td, ^3J = 7.8 Hz, ^4J = 1.7 Hz), 8.52 (2H, d, ^3J = 5.1 Hz), 10.40 (1H, s, broad). ^{13}C NMR (75 MHz, $CDCl_3$): δ = 24.5 (CH_3), 29.9 (3 CH_3), 35.4 (C), 56.3 (CH_3), 58.2 (CH_2), 59.7 (2 CH_2), 112.7 (CH), 1313.4 (CH), 120.5 (CH), 122.1 (CH), 122.5 (CH), 123.6 (C), 123.9 (CH), 136.9 (CH), 137.1 (CH), 138.2 (C), 149.3 (CH), 150.8 (C), 151.8 (C), 157.8 (C), 158.4 (C), 158.8 (C). MS (DCI, NH_3/isobutane): *m*/*z* (%) 406 (100) $[M + H]^+$. Anal. Calcd for $C_{25}H_{31}N_3O_2$: C, 74.04; H, 7.70; N, 10.36. Found: C, 72.26; H, 7.63; N, 10.36%.

5L. This ligand was prepared in a similar way as 4H, by using the 2-*tert*-butyl-4-fluoro-phenol instead of the 2-*tert*-butyl-4-methoxy-phenol. Column chromatography on silica gel (ethyl acetate–pentane (2/8)) yielded 5L (40%) as a pale yellow oil. ^{1}H NMR (400 MHz, $CDCl_3$): δ = 1.44 (9H, s), 2.59 (3H, s), 3.74 (2H, s), 3.83 (2H, s), 3.84 (2H, s), 6.63 (1H, dd, ^3J = 8.1 Hz, ^4J = 3.1 Hz), 6.90 (1H, dd, ^3J = 11.1 Hz, ^4J = 3.1 Hz), 7.01 (1H, d, ^3J = 7.6 Hz), 7.07 (1H, d, ^3J = 7.6 Hz), 7.13 (1H, dd, ^3J = 7.0 Hz, ^4J = 5.0 Hz), 7.36 (1H, d, ^3J = 7.8 Hz), 7.50 (1H, t, ^3J = 7.8 Hz), 7.60 (1H, td, ^3J = 7.8 Hz, ^4J = 1.8 Hz), 8.53 (1H, d, ^3J = 4.7 Hz), 10.70 (1H, s, broad). ^{13}C NMR (100 MHz, $CDCl_3$): δ = 24.4 (CH_3), 29.7 (3 CH_3), 35.3 (C), 57.6 (CH_2), 59.6 (CH_2), 59.8 (CH_2), 113.1 (CH), 114.1 (CH), 120.4 (CH), 122.1 (CH), 122.5 (CH), 123.8 (CH), 124.0 (C), 136.9 (CH), 137.2 (CH), 138.6 (C), 149.3 (CH), 156.9 (C), 157.5 (C), 158.4 (C), 158.6 (C). MS (DCI, NH_3/isobutane): *m*/*z* (%) 394 (100) $[M + H]^+$. Anal. Calcd for $C_{24}H_{28}FN_3O$: C, 73.26; H, 7.17; N, 10.68. Found: C, 74.01; H, 7.22; N, 10.52%.

6L. This ligand was prepared in a similar way as 4L, by using bis-(6-methyl-pyridin-2-ylmethyl)-amine[61] instead of (6-methyl-pyridin-2-ylmethyl)-pyridin-2-ylmethyl-amine. Column chromatography on silica gel (ethyl acetate–pentane (2/8)) yielded 6L (40%) as a pale yellow oil. ^{1}H NMR (400 MHz, $CDCl_3$): δ = 1.45 (9H, s), 2.56 (6H, s), 3.73 (3H, s), 3.74 (2H, s), 3.82 (4H, s), 6.48 (1H, d, ^4J = 3.1 Hz), 6.79 (1H, d, ^4J = 3.2 Hz), 7.00 (2H, d, ^3J = 7.6 Hz), 7.15 (2H, d, ^3J = 7.6 Hz), 7.49 (1H, t, ^3J = 7.9 Hz), 10.40 (1H, s, broad). ^{13}C NMR (100 MHz, $CDCl_3$): δ = 24.5 (CH_3), 29.7 (3 CH_3), 35.2 (C), 56.0 (CH_3), 58.0 (CH_2), 59.7 (2 CH_2), 112.6 (CH), 113.3 (CH), 120.4 (CH), 121.9 (CH), 123.6 (C), 137.0 (CH), 138.0 (C), 150.7 (C), 151.8 (C), 157.9 (C), 158.0 (C). MS (DCI, NH_3/isobutane): *m*/*z* (%) 420 (100) $[M + H]^+$. Anal. Calcd for $C_{26}H_{33}N_3O_2$: C, 74.43; H, 7.93; N, 10.02. Found: C, 74.36; H, 7.81; N, 10.06%.

1·(ClO$_4$)$_2$. 1L (54.6 mg, 0.163 mmol) was dissolved in methanol (3 mL) and then $Cu(ClO_4)_2{\cdot}6H_2O$ (60.3 mg, 0.163 mmol in a methanolic solution) and NEt_3 (22.8 µl, 0.163 mmol ml) were added. The solution was stirred for 10 min at room temperature, left to evaporate overnight, and then stored for 10 h at 253 K. A dark brown precipitate of **1·(ClO$_4$)$_2$** was formed, which was collected by filtration (50 mg, 31% yield). Slow diffusion of diethyl ether into a concentrated CH_3CN solution of the complex affords brown single crystals of **1·(ClO$_4$)$_2$·(CH$_3$CN)$_4$**. MS (ESI, CH_3CN): *m*/*z* (%) 396 (100) $[M_{0.5} - 2ClO_4]^+$. Anal. Calcd for $C_{40}H_{40}Cl_2Cu_2N_6O_{12}$: C, 48.30; H, 4.05; N, 8.45. Found: C, 48.52; H, 4.03; N, 8.35. UV-Vis (λ_{max} [nm] [ε/M^{-1} cm^{-1}] in CH_3CN, 298 K): 466 [1015], 853 [670].

3·ClO$_4$. 3L (170 mg, 0.419 mmol) was dissolved in CH_3CN (3 mL) and then $Cu(ClO_4)_2{\cdot}6H_2O$ (156 mg, 0.412 mmol) was added. The solution was stirred for 30 min. Slow diffusion of diisopropyl ether into the resulting solution affords blue single crystals of **3·ClO$_4$** (237 mg, 80% yield). MS (ESI, CH_3CN): *m*/*z* (%) 467 (100) $[M - H - 2ClO_4 - CH_3CN]^+$. Anal. Calcd for $C_{27}H_{34}Cl_2CuN_4O_{10}$: C, 45.74; H, 4.83; N, 7.90. Found: C, 45.82; H, 4.83; N, 7.90. UV-Vis (λ_{max} [nm] [ε/M^{-1} cm^{-1}] in CH_3CN, 298 K): 573 [230].

Complexes **4·ClO$_4$** and **5·ClO$_4$** were prepared in an identical manner in 80 and 63% yield respectively. **6**$^+$ was prepared *in situ* in its phenolate form by mixing equimolar amounts of 6L and $Cu(ClO_4)_2{\cdot}6H_2O$ in DMF.

4·ClO$_4$. MS (ESI, CH_3CN): *m*/*z* (%) 467 (100) $[M - H - 2ClO_4 - CH_3CN]^+$. Anal. Calcd for $C_{27}H_{34}Cl_2CuN_4O_{10}$: C, 45.74; H, 4.83; N, 7.90. Found: C, 45.50; H, 4.77; N, 7.86. UV-Vis (λ_{max} [nm] [ε/M^{-1} cm^{-1}] in CH_3CN, 298 K): 590 [210].

5·ClO$_4$. MS (ESI, CH_3CN): *m*/*z* (%) 455 (100) $[M - H - 2ClO_4 - CH_3CN]^+$. Anal. Calcd for $C_{26}H_{31}Cl_2CuFN_4O_9$: C, 44.80; H, 4.48; N, 8.04. Found: C, 44.51; H, 4.39; N, 7.90. UV-Vis (λ_{max} [nm] [ε/M^{-1} cm^{-1}] in CH_3CN, 298 K): 622 [100].

6$^+$ in DMF solution (phenolate cationic form with a coordinated DMF molecule). MS (ESI, DMF–H_2O): *m*/*z* (%) 481.2 (30) $[M - DMF]^+$, 482.2 (70) $[M + H - DMF]^+$ (this copper(I) form of the complex results from the reduction of **6**$^+$ in the gas phase).[62] EPR (100 K, DMF): $g_{xx} = g_{yy} = 2.057$, $g_{zz} = 2.265$, $A_{xx\ (Cu)} = A_{yy\ (Cu)} = 1.5$ mT, $A_{zz\ (Cu)} = 15.7$ mT; UV-Vis (λ_{max} [nm] [ε/M^{-1} cm^{-1}] in DMF, 298 K): 543 [975].

Determination of the DNA binding constants

The DNA binding constants were obtained from titration of solutions of the complexes with CT DNA. DNA (type I, fibers, from Sigma Aldrich) was first purified by four successive extractions with the phenol–$CHCl_3$–isoamyl alcohol 25–24–1 mixture. Then 0.1 volume (with respect to the aqueous phase) of a 3 M sodium acetate solution and 2 volumes of ethanol were added and the solution was stored overnight at 253 K. The precipitated DNA was solubilised and analyzed by UV-Vis to ensure that the A_{260}/A_{280} ratio was ≥2. In a typical titration experiment 50 µl of a stock solution of the complex in DMF (0.5–1 mM) was mixed with 20 µl of phosphate buffer (50 mM) at pH 7.3, and 430 µl of an aqueous solution of CT DNA (concentration ranging from 0 to 0.5 mM) was added. After the equilibrium was reached (10 min) at 298 K the UV-Vis spectrum of the solution was recorded. The DNA binding constants K_b were calculated using the equation:

$$[DNA]/(\varepsilon_a - \varepsilon_f) = [DNA]/(\varepsilon_b - \varepsilon_f) + 1/K_b$$

where ε_a is the apparent molar extinction coefficient of the complex at a given DNA concentration, ε_f is the molar extinction coefficient of the free complex, and ε_b is the molar extinction coefficient of fully bound complex. A plot of $[DNA]/(\varepsilon_a - \varepsilon_f)$ as a function of DNA concentration gives a straight line whose slope is $1/(\varepsilon_b - \varepsilon_f)$ and the *Y*-intercept is equal to $1/K_b(\varepsilon_b - \varepsilon_f)$. Each binding constant was obtained from a triplicate experiment.

Procedure for DNA cleavage experiments

ϕX174 RF1 DNA was purchased from Fermentas and was stored at −20 °C. The typical reaction mixture, containing double-stranded DNA and the Cu^{II} complexes in a 10 mM phosphate solution (pH 7.2 or 8.2) with 10% DMF, was incubated at 37 °C for the required time, with or without additives. After the incubation period, the reaction was quenched at −20 °C, followed by the addition of loading buffer (6× loading dye solution, Fermentas). The reaction mixture was loaded on a 0.8% agarose gel in Tris–Boric acid–EDTA buffer (pH 8.2) (0.5× TBE) and electrophoresis was performed at 70 V for 2 h 30 min–3 h. After DNA migration, the gels were stained by incubation for 10 min with a 1 µg ml^{-1} ethidium bromide (EB) solution and then washed with distilled water. The gels were visualised and the fluorescence was quantified using Imager Typhoon 9400 and Image Quant software. The cleavage efficiency was measured by determining the ability of the complex to convert the supercoiled DNA (SC) to nicked circular form (NC) and linear form (L). For kinetic analysis we determined the amounts of SC and NC forms on the agarose gel by image processing with imageJ 1.46r freeware (Wayne Rasband National Institute of Health, USA). The data were then refined by simplex algorithm by considering a mono-exponential function (commercial Bio-kine 4.44 software, Biologic Co., Le Pont-de-Claix, France).

Enzymatic religation assays

The supercoiled DNA was treated with the copper complexes at 37 °C and pH 7.2. DNA samples were purified over QIAquick PCR purification columns (Qiagen) and were used for religation experiments. Ligation was performed in 25 μL with 2.5 μL of 10× ligation buffer and 2 units of T4 ligase (Fermentas) for 16 h at 16 °C. Similarly, and for comparison, the supercoiled DNA was digested using XhoI restriction enzyme (Fermentas) and religated using the above procedure, and found 100% religation.

Cell culture

Human bladder cancer cell line RT112 was obtained from Cell Lines Service (Eppelheim, Germany). Cisplatin resistant RT112 cells (RT112-CP) were kindly provided by B. Köberle (Institute of Toxicology, Clinical Centre of University of Mainz, Mainz, Germany). RT112 and RT112-CP cells were cultured in RPMI 1640 medium supplemented with 10% (v/v) fetal calf serum (FCS) and 2 mM glutamine (Invitrogen Life Technologies, Paisley, UK). Cells were maintained at 37 °C in a 5% CO_2-humidified atmosphere and tested to ensure freedom from mycoplasma contamination.

Cell proliferation assay

Inhibition of cell proliferation by copper complexes was measured by a MTT (3-(4,5-dimethylthiazol-2-yl)-2,5-diphenyltetrazolium bromide) assay. RT112 and RT112-CP cells were seeded into 96-well plates (5×10^3 cells per well) in 100 μl of culture medium. After 24 h, cells were treated with cisplatin (Sigma-Aldrich, Lyon, France) or complexes $\mathbf{1}^{2+}$–$\mathbf{6}^{+}$ at various concentrations. In parallel, a control with DMSO (vehicle alone) at the same dilutions was done. Following incubation for 48 h, 10 μl of a MTT (Euromedex, Mundolsheim, France) stock solution in PBS at 5 mg ml^{-1} was added in each well and the plates were incubated at 37 °C for 3 h. Plates were then centrifugated for 5 min at 400 g before the medium was discarded and replaced with DMSO (100 μl per well) to solubilize water-insoluble purple formazan crystals. After 15 min under shaking, absorbance was measured on an ELISA reader (Tecan, Männedorf, Switzerland) at a test wavelength of 570 nm and a reference wavelength of 650 nm. Absorbance obtained by cells treated with the same dilution of the vehicle alone (DMSO) was rated as 100% cell survival. Each data point is the average of three independent experiments.

Cell cycle analysis

RT112 cells were cultured in 6-well plates (2×10^5 cells per well) for 24 h before treatment with DMSO or complexes $\mathbf{2}^{+}$, $\mathbf{4}^{+}$, $\mathbf{5}^{+}$ and $\mathbf{6}^{+}$ for 24 h or 48 h. Trypsinized and floating cells were then pooled, fixed with 70% ethanol, washed with PBS and stained with 20 μg ml^{-1} propidium iodide (PI) in the presence of 0.5 mg ml^{-1} of RNAse (Sigma-Aldrich, Lyon, France). Data acquisitions were performed with a FACScan (Becton Dickinson France, Le Pont-de-Claix, France) equipped with a 488 nm argon laser and PI fluorescence was collected with a 585 ± 44 nm filter. Parameters from 2×10^4 cells were acquired using Cell Quest Pro software (Becton Dickinson). The percentage of cell cycle distribution in the G1, S and G2 + M phases was determined using FCS Express 3 software (De Novo Sofware, Los Angeles, CA).

Acknowledgements

We thank the Labex Arcane (Université Joseph Fourier, Grenoble) and the Association Espoir and GEFLUC (Délégation de l'Isère) for financial support.

Notes and references

1 G. J. Brewer, *Exp. Biol. Med.*, 2001, **226**, 665.
2 T. Theophanides and J. Anastassopoulou, *Crit. Rev. Oncol. Hematol.*, 2002, **42**, 57; X. Zhang, C. Bi, Y. Fan, Q. Cui, D. Chen, Y. Xiao and Q. Ping Dou, *Int. J. Mol. Med.*, 2008, **22**, 677; C. Marzano, M. Pellei, F. Tisano and C. Santini, *Anti-Cancer Med. Chem.*, 2009, **9**, 185; S. Tardito and L. Marchio, *Curr. Med. Chem.*, 2009, **16**, 1325.
3 A. Chan, F. Wong and M. Arumanayagam, *Ann. Clin. Biochem.*, 1993, **30**, 545; M. Zowczak, M. Iskra, L. Torlinski and S. Cofta, *Biol. Trace Elem. Res.*, 2001, **82**, 1.
4 H. Mazdak, F. Yazdekhasti, A. Movahedian, N. Mirkheshti and M. Shafieian, *Int. Urol. Nephrol.*, 2010, **42**, 89.
5 S. Majumder, S. Chatterjee, S. Pal, J. Biswas, T. Efferth and S. K. Choudhuri, *Biometals*, 2009, **22**, 377.
6 S. Adsule, V. Barve, D. Chen, F. Ahmed, Q. P. Dou, S. Padhye and F. H. Sarkar, *J. Med. Chem.*, 2006, **49**, 7242.
7 E. Wong and C. M. Giandomenico, *Chem. Rev.*, 1999, **99**, 2451; E. R. Jamieson and S. J. Lippard, *Chem. Rev.*, 1999, **99**, 2467; J. Reedijk, *Eur. J. Inorg. Chem.*, 2009, 1303.
8 A. M. Angeles-Boza, P. M. Bradley, P. K. L. Fu, S. E. Wicke, J. Bacsa, K. M. Dunbar and C. Turro, *Inorg. Chem.*, 2004, **43**, 8510; T. Tanaka, K. Yukawa and N. Umesaki, *Oncol. Rep.*, 2005, **14**, 1365; D. Wang and S. J. Lippard, *Nat. Rev. Drug Discovery*, 2005, **4**, 307.
9 A. Q. Lei, L. Cheng and C.-X. Pan, *Expert Rev. Anticancer Therapy*, 2011, **11**, 1851.
10 B. Meunier, *Chem. Rev.*, 1992, **92**, 1411; D. S. Sigman, *Acc. Chem. Res.*, 1986, **19**, 180; G. Jiang, N. Xiao, P. Shi, Y. Zhu and Z. Guo, *Coord. Chem. Rev.*, 2007, 1951; M. Pitié and G. Pratviel, *Chem. Rev.*, 2010, **110**, 1018.
11 L. Li, N. N. Murthy, J. Telser, L. N. Zakharov, G. P. A. Yap, A. L. Rheingold, K. D. Karlin and S. E. Rokita, *Inorg. Chem.*, 2006, **45**, 7144.
12 For recent representative articles see: S. Thyagarajan, N. N. Murthy, A. A. Narducci Sarjeant, K. D. Karlin and S. E. Rokita, *J. Am. Chem. Soc.*, 2006, **128**, 7003; J. L. Garcia-Gimenez, G. Alzuet, M. Gonzales-Alvarez, A. Castinheiras, M. Liu-Gonzalez and J. Borras, *Inorg. Chem.*, 2007, **46**, 7178; M. Gonzales-Alvarez, G. Alzuet, J. Borras, L. des Castillo-Agudo, J. M. Montejo-Bernardo, A. Gutierrez-

Rodriguez and S. Garcia-Granda, *J. Biol. Inorg. Chem.*, 2008, **13**, 1249; Y. Kou, J. Tian, D. Li, W. Gu, X. Liu, S. Yan, D. Liao and P. Cheng, *Dalton Trans.*, 2009, 2374; A. Arbuse, M. Font, M. A. Martinez, X. Fontrodona, M. J. Prieto, V. Moreno, X. Sala and A. Llobet, *Inorg. Chem.*, 2009, **48**, 11098; K. Ghosh, P. Kumar, N. Tyagi, U. P. Singh, V. Aggarwal and M. C. Baratto, *Eur. J. Med. Chem.*, 2010, **45**, 3770.

13 S. Dhar, M. Nethaji and A. R. Chakravarty, *Inorg. Chem.*, 2005, **44**, 8876.

14 S. Dhar, M. Nethaji and A. R. Chakravarty, *Inorg. Chim. Acta*, 2005, **358**, 2437; S. Dhar, M. Nethaji and A. R. Chakravarty, *Inorg. Chem.*, 2006, **45**, 11043.

15 M. Scarpellini, A. Neves, R. Horner, A. J. Bortoluzzi, B. Szpoganics, C. Zucco, R. A. Nome Silva, V. Drago, A. S. Mangrich, W. A. Ortiz, W. A. C. Passos, M. C. B. De Oliveira and H. Terenzi, *Inorg. Chem.*, 2003, **42**, 8353; C. Fernande, G. L. Parrilha, J. A. Lessa, L. J. M. Santiago, M. M. Kanashiro, F. S. Boniolo, A. J. Bortoluzzi, N. V. Vugman, M. H. Herbst and A. Horn Jr., *Inorg. Chim. Acta*, 2006, **359**, 3167.

16 M. C. B. Oliveira, D. Mazera, M. Scarpellini, P. Cardoso Severino, A. Neves and H. Terenzi, *Inorg. Chem.*, 2009, **48**, 2711.

17 V. Rajendiran, R. Karthik, M. Palaniandavar, H. Stoeckli-Evans, V. S. Periasamy, M. A. Akbarsha, B. S. Srinag and H. Krishnamurthy, *Inorg. Chem.*, 2007, **46**, 8208.

18 S. Ramakrishnan, V. Rajendiran, M. Palaniandavar, V. S. Periasamay, M. A. Akbarsha, B. S. Srinag and H. Krishnamurthy, *Inorg. Chem.*, 2009, **48**, 1309; R. Loganathan, S. Ramakrishnan, E. Suresh, A. Riyasdeen, M. A. Akbarsha and M. Palaniandavar, *Inorg. Chem.*, 2012, **51**, 5512.

19 S. Borah, M. S. Melvin, N. Lindquist and R. A. Manderville, *J. Am. Chem. Soc.*, 1998, **120**, 4557; M. S. Melvin, J. T. Tomlinson, G. R. Saluta, G. L. Kucera, N. Lindquist and R. A. Manderville, *J. Am. Chem. Soc.*, 2000, **122**, 6333.

20 T. Bortolotto, P. Pereira Silva, A. Neves, E. C. Pereira-Maia and H. Terenzi, *Inorg. Chem.*, 2011, **50**, 10519.

21 S. S. Bhat, A. A. Kumbhar, H. Heptullah, A. A. Khan, V. V. Gobre, S. P. Gejji and V. G. Puranik, *Inorg. Chem.*, 2011, **50**, 545.

22 P. U. Maheswari, S. Roy, H. Den Dulk, S. Barends, G. Van Wezel, B. Kozlevcar, P. Gamez and J. Reedijk, *J. Am. Chem. Soc.*, 2006, **128**, 710; P. U. Maheswari, S. Barends, S. Özalp-Yaman, P. De Hoog, H. Casellas, S. J. Teat, C. Massera, M. Lutz, A. L. Spek, G. P. Van Wezel, P. Gamez and J. Reedijk, *Chem.–Eur. J.*, 2007, **13**, 5213; S. Roy, P. U. Maheswari, M. Lutz, A. L. Spek, H. den Dulk, S. Barends, G. P. van Wezel, F. Hartlc and J. Reedijk, *Dalton Trans.*, 2009, 10846.

23 K. Ghosh, P. Kumar, N. Tyagi and U. P. Singh, *Inorg. Chem.*, 2010, **49**, 7614; K. Ghosh, P. Kumar, V. Mohan, U. P. Singh, S. Kasiri and S. S. Mandal, *Inorg. Chem.*, 2012, **51**, 3343.

24 A. Philibert, F. Thomas, C. Philouze, S. Hamman, E. Saint-Aman and J. L. Pierre, *Chem.–Eur. J.*, 2003, **9**, 3803.

25 F. Michel, F. Thomas, S. Hamman, E. Saint-Aman, C. Bucher and J. L. Pierre, *Chem.–Eur. J.*, 2004, **10**, 4115.

26 A. W. Addison, T. N. Rao, J. Reedijk, J. Von Rijn and G. C. Verschoor, *J. Chem. Soc., Dalton Trans.*, 1984, 1349.

27 D. Zurita, I. Gautier-Luneau, S. Ménage, J. L. Pierre and E. Saint-Aman, *J. Biol. Inorg. Chem.*, 1997, **2**, 46; S. Itoh, S. Takayama, R. Arakawa, A. Furuta, M. Komatsu, A. Ishida, S. Takamuku and S. Fukuzumi, *Inorg. Chem.*, 1997, **36**, 1407; Y. Shimazaki, S. Huth, A. Odani and O. Yamauchi, *Angew. Chem., Int. Ed.*, 2000, **39**, 1666; F. Thomas, G. Gellon, I. Gautier-Luneau, E. Saint-Aman and J.-L. Pierre, *Angew. Chem., Int. Ed.*, 2002, **41**, 3044.

28 S. Itoh, M. Taki, H. Kumei, S. Takayama, S. Nagatomo, T. Kitagawa, N. Sakurada, R. Arakawa and S. Fukuzumi, *Inorg. Chem.*, 2000, **39**, 3708.

29 Y. Shimazaki, S. Huth, S. Hirota and O. Yamauchi, *Bull. Chem. Soc. Jpn.*, 2000, **73**, 1187.

30 C. G. Saysell, C. D. Borman, A. J. Baron, M. J. McPherson and A. G. Sykes, *Inorg. Chem.*, 1997, **36**, 4520.

31 F. Michel, F. Thomas, S. Hamman, C. Philouze, E. Saint-Aman and J. L. Pierre, *Eur. J. Inorg. Chem.*, 2006, 3684.

32 F. Michel, S. Hamman, F. Thomas, C. Philouze, I. Gautier-Luneau and J. L. Pierre, *Chem. Commun.*, 2006, 4122; F. Michel, S. Hamman, C. Philouze, C. Pérez Del Valle, E. Saint-Aman and F. Thomas, *Dalton Trans.*, 2009, 832.

33 H. Adams, N. A. Bailey, I. K. Campbell, D. E. Fenton and H. YU He, *J. Chem. Soc., Dalton Trans.*, 1996, 2233.

34 M. Vaidyanathan, R. Viswanathan, M. Palaniandavar, T. Balasubramanian, P. Prabhaharan and T. P. Muthiah, *Inorg. Chem.*, 1998, **37**, 6418.

35 H. Adams, N. A. Bailey, C. O. Rodriguez de Barbarin, D. E. Fenton and Q. Y. He, *J. Chem. Soc., Dalton Trans.*, 1995, 2323.

36 P. Kumar, S. Gorai, M. K. Santra, B. Mondal and D. Manna, *Dalton Trans.*, 2012, **41**, 7573.

37 M. C. B. De Oliveira, M. Scarpellini, A. Neves, H. Terenzi, A. J. Bortoluzzi, B. Szpoganics, A. Greatti, A. S. Mangrich, E. M. de Souza, P. M. Fernadez and M. R. Soares, *Inorg. Chem.*, 2005, **44**, 921.

38 R. H. Wopschall and I. Shain, *Anal. Chem.*, 1967, **39**, 1514.

39 H. Nagao, N. Komeda, M. Mukaida, M. Suzuki and K. Tanaka, *Inorg. Chem.*, 1996, **35**, 6809.

40 M. Schatz, M. Becker, F. Thaler, F. Hampel, S. Schindler, R. R. Jacobson, Z. Tyeklar, N. N. Murthy, P. Ghosh, Q. Chen, J. Zubieta and K. D. Karlin, *Inorg. Chem.*, 2001, **40**, 2312; W. Canõn-Mancisidor, E. Spodine, D. Venegas-Yazigi, D. Rojas, J. Manzur and S. Alavarez, *Inorg. Chem.*, 2008, **47**, 3687.

41 F. Thomas, O. Jarjayes, C. Duboc, C. Philouze, E. Saint-Aman and J.-L. Pierre, *Dalton Trans.*, 2004, 2662.

42 L. Zhu, O. dos Santos, C. W. Koo, M. Rybstein, L. Pape and J. W. Canary, *Inorg. Chem.*, 2003, **42**, 7912.

43 S. I. Kirin, C. M. Happel, S. Hrubanova, T. Weyhermueller, C. Klein and N. Metzler-Nolte, *Dalton Trans.*, 2004, 1201.

44 Y. An, S.-D. Liu, S.-Y. Deng, L.-N. Ji and Z.-W. Mao, *J. Inorg. Biochem.*, 2006, **100**, 1586.

45 Y. Shao, X. Sheng, Y. Li, Z.-L. Jia, J.-J. Zhang, F. Liu and G.-Y. Lu, *Bioconjugate Chem.*, 2008, **19**, 1840.
46 L. Tjioe, A. Meininger, T. Joshi, L. Spiccia and B. Graham, *Inorg. Chem.*, 2011, **50**, 4327.
47 A. Barve, A. Kumbhar, M. Bhat, B. Joshi, R. Butcher, U. Sonawane and R. Joshi, *Inorg. Chem.*, 2009, **48**, 9120.
48 M. Tian, H. Ihmals and E. Brötz, *Dalton Trans.*, 2010, **39**, 8195.
49 C. Liu, S. Yu, D. Li, Z. Liao, X. Sun and H. Xu, *Inorg. Chem.*, 2002, **41**, 913.
50 C. Liu, S. Yu, D. Li, Z. Liao, X. Sun and H. Xu, *Inorg. Chem.*, 2002, **41**, 913.
51 F. M. Muggia and T. Fojo, *J. Chemotherapy*, 2004, **4**, 77.
52 P. Falco, S. Bringhen, I. Avonto, F. Gay, F. Morabito, M. Boccadoro and A. Palumbo, *Expert Rev. Anticancer Ther.*, 2007, **7**, 945.
53 D. Catovsky, M. Else and S. Richards, *Clin. Lymphoma Myeloma Leuk.*, 2011, **11**, S2.
54 M. Froudarakis, E. Hatzimichael, L. Kyriazopoulou, K. Lagos, P. Pappas, A. Tzakos, V. Karavasilis, D. Daliani, C. Papandreou and E. Briasoulis, *Crit. Rev. Oncol. Hematol.*, 2013, DOI: 10.1016/j.critrevonc.2012.12.003, ASAP.
55 D. C. Marks, L. Belov, M. W. Davey, R. A. Davey and A. D. Kidman, *Leuk. Res.*, 1992, **16**, 1165.
56 D. J. Gallagher and M. I. Milowsky, *Curr. Treat. Options Oncol.*, 2009, **10**, 205.
57 B. Köberle, J. Payne, K. A. Grimaldi, J. A. Hartley and J. R. Masters, *Biochem. Pharmacol.*, 1996, **52**, 1729.
58 J. R. Jackson, A. Gilmartin, C. Imburgia, J. D. Winkler, L. A. Marshall and A. Roshak, *Cancer Res.*, 2000, **60**, 566; R. S. DiPoala, *Clin. Cancer Res.*, 2002, **8**, 3311.
59 J. H. Houtgraaf, J. Versmissen and W. J. van der Giessen, *Cardiovasc. Revasc. Med.*, 2006, **7**, 165.
60 O. V. Dolomanov, L. J. Bourhis, R. J. Gildea, J. A. K. Howard and H. Puschmann, *J. Appl. Crystallogr.*, 2009, **42**, 339.
61 H. Nagao, N. Komeda, M. Mukaida, M. Suzuki and K. Tanaka, *Inorg. Chem.*, 1996, **35**, 6809.
62 L. Gianelli, V. Amendola, L. Fabbrizzi, P. Pallavicini and G. G. Mellerio, *Rapid Commun. Mass Spectrom.*, 2001, **15**, 2347.